Recent developments in the modelling of neutron-star crusts

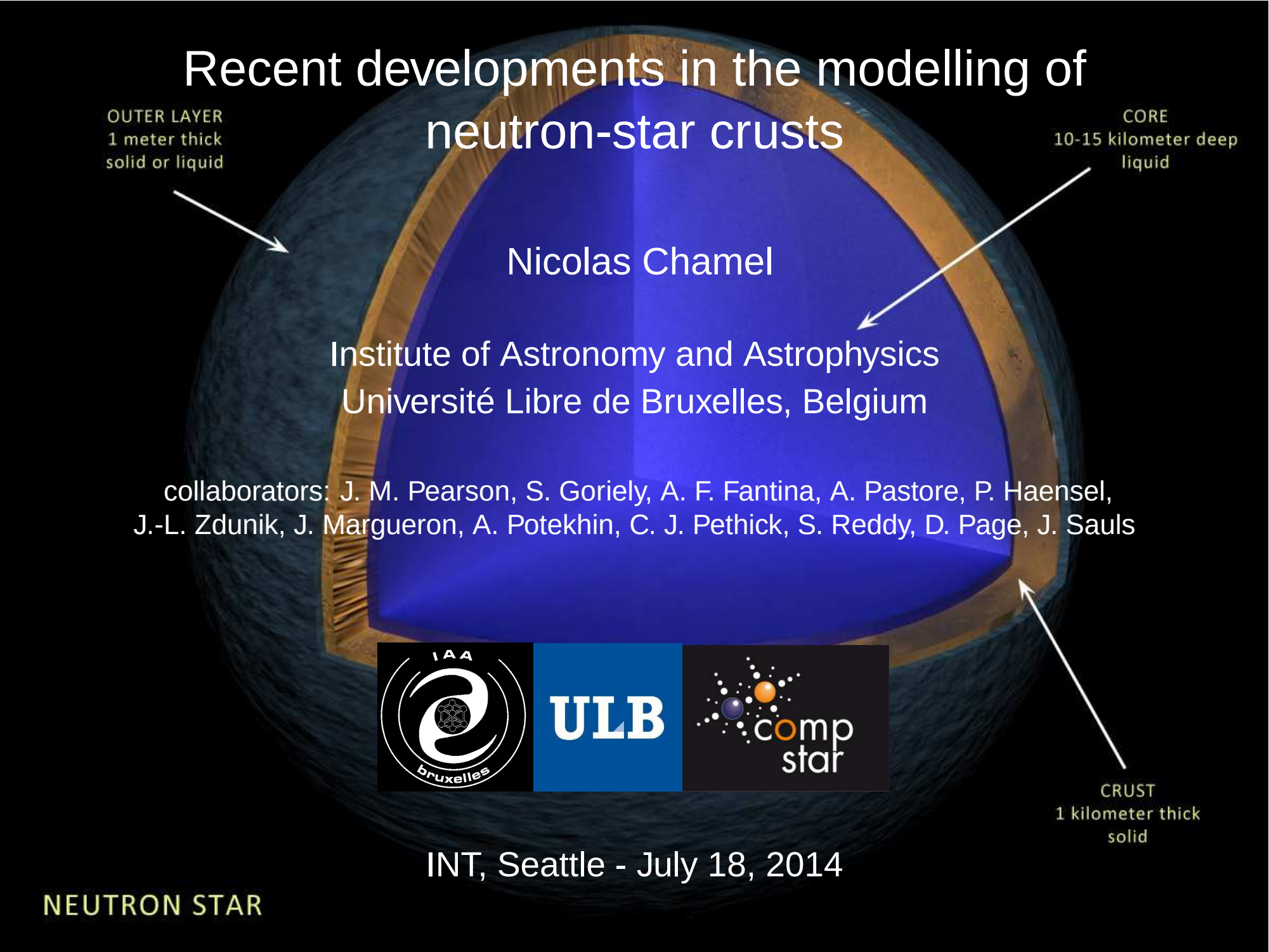

Nicolas Chamel

Institute of Astronomy and Astrophysics
Université Libre de Bruxelles, Belgium

collaborators: J. M. Pearson, S. Goriely, A. F. Fantina, A. Pastore, P. Haensel, J.-L. Zdunik, J. Margueron, A. Potekhin, C. J. Pethick, S. Reddy, D. Page, J. Sauls

INT, Seattle - July 18, 2014

Punchline

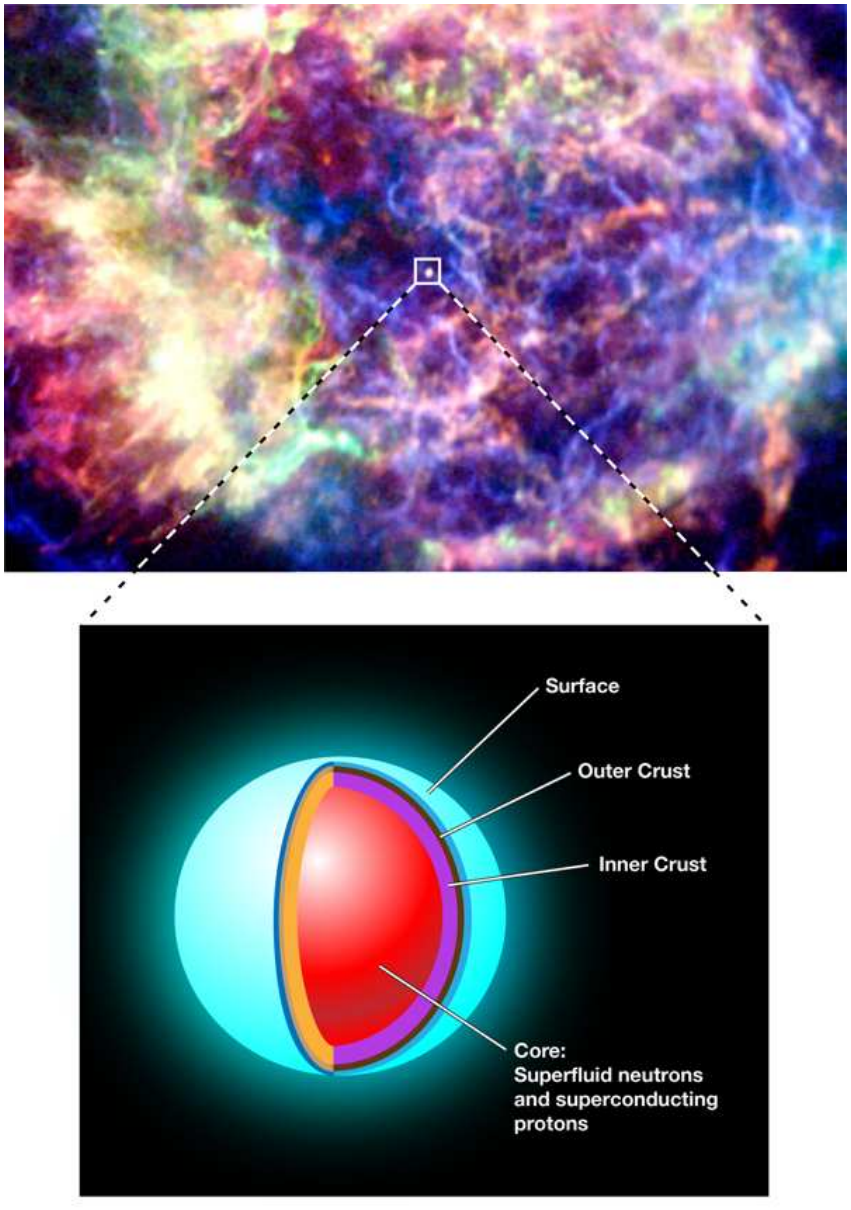

Even though the crust of a neutron star represents about $\sim 1\%$ of the stellar mass and $\sim 10\%$ of the stellar radius, it is thought to be related to various observed phenomena:

- pulsar glitches,
- X-ray bursts and superbursts,
- deep crustal heating,
- thermal relaxation in SXT,
- QPOs in SGR, etc.

Challenge

Although the crust is made of neutrons, protons and electrons, it exhibits very different phases of matter:

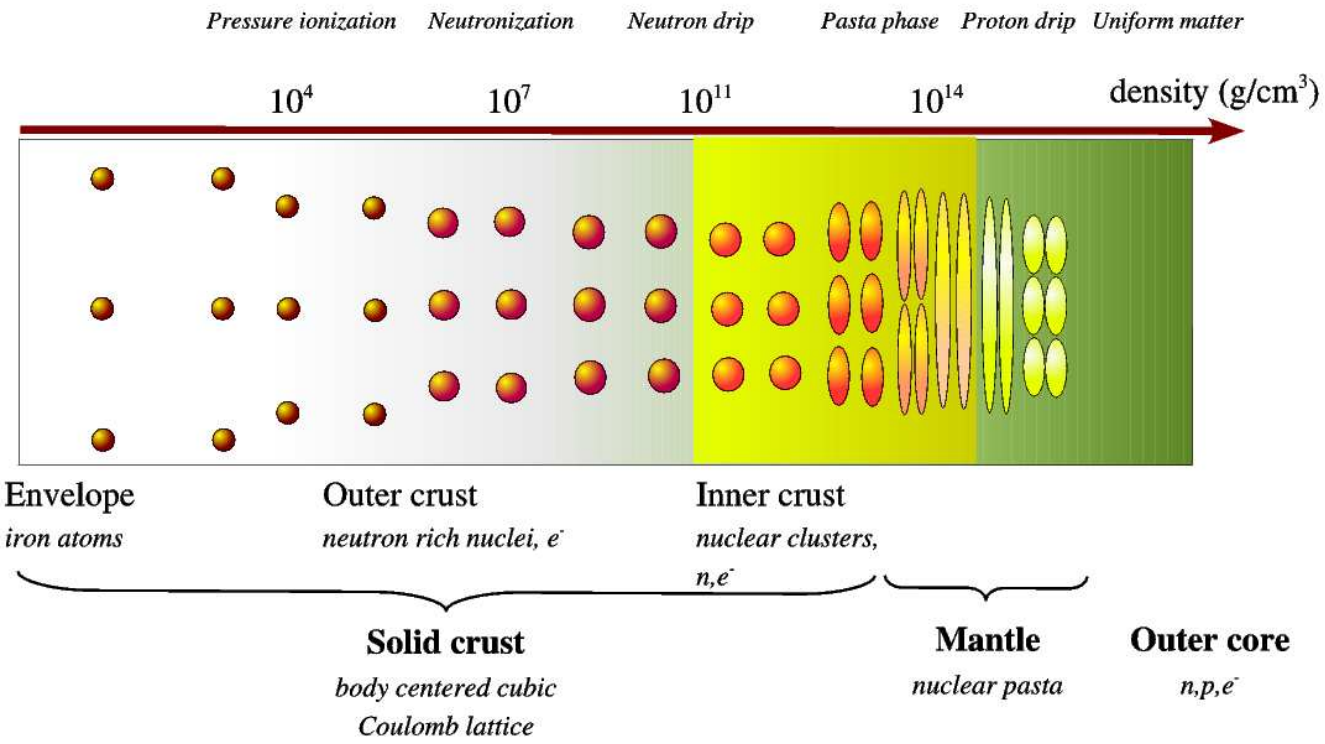

Our goal is to describe all these phases in a *unified* and *consistent* way using the *same* nuclear model.

Outline

1. Effective nuclear models
2. Structure and composition of neutron-star crusts
3. Superfluidity
4. Collective excitations and thermal properties

Effective nuclear models

Nuclear energy density functional theory in a nut shell

This theory allows for a **tractable and consistent** treatment of atomic nuclei and nuclear matter in compact stars.

What is it all about ?

The energy of a lump of matter is expressed as ($q = n, p$)

$E = \int \mathrm{d}^3\boldsymbol{r}\, \mathcal{E}\Big[\rho_q(\boldsymbol{r}), \boldsymbol{\nabla}\rho_q(\boldsymbol{r}), \tau_q(\boldsymbol{r}), \boldsymbol{J}_q(\boldsymbol{r})\Big]$ where $\rho_q(\boldsymbol{r})$, $\tau_q(\boldsymbol{r})$ and $\boldsymbol{J}_q(\boldsymbol{r})$ are functionals of wavefunctions $\varphi^{(q)}(\boldsymbol{r})$ obeying

$$\left[-\boldsymbol{\nabla}\cdot\frac{\delta E}{\delta\tau_q}\boldsymbol{\nabla} + \frac{\delta E}{\delta\rho_q} - \mathrm{i}\frac{\delta E}{\delta \boldsymbol{J}_q}\cdot\boldsymbol{\nabla}\times\boldsymbol{\sigma}\right]\varphi^{(q)} = \varepsilon^{(q)}\varphi^{(q)}\,.$$

This scheme can be extended to account for pairing (HFB).

Problem: we don't know what the functional E is... Therefore, we use **phenomenological functionals**.

Thermodynamic variables vs nuclear parameters

Two different kinds of parameters should be distinguished:

- **thermodynamic variables**, related to the physical conditions prevailing in the star
  e.g. pressure, temperature, magnetic field, *etc.*
- **nuclear parameters** characterizing nuclear matter
  e.g. energy per nucleon of nuclear matter at $T = 0$ around saturation density n_0 and for asymmetry $\eta = (n_n - n_p)/n$

  $e(n, \eta) = e_0(n) + S(n)\eta^2 + o\left(\eta^4\right)$ where

  $e_0(n) = a_v + \frac{K_v}{18}\epsilon^2 - \frac{K'}{162}\epsilon^3 + o\left(\epsilon^4\right)$ with $\epsilon = (n - n_0)/n_0$

  $S(n) = J + \frac{L}{3}\epsilon + \frac{K_{sym}}{18}\epsilon^2 + o\left(\epsilon^3\right)$ is the symmetry energy

The nuclear parameters are known with some uncertainties.
This is reflected in the existence of many different functionals.

Which functional should we choose?

The nuclear energy density functional theory has been very successfully applied to describe the structure and the dynamics of medium-mass and heavy nuclei.

However, most functionals are not suitable for neutron stars:

- they were adjusted to a few selected nuclei (mostly with equal numbers of neutrons and protons)
- they yield unrealistic neutron-matter EoS
- they yield unrealistic pairing gaps in nuclear matter
- they yield unrealistic effective masses
- they lead to spurious instabilities in nuclear matter (e.g. ferromagnetic transition).

Brussels-Montreal Skyrme functionals (BSk)

These functionals were fitted to both experimental data and N-body calculations using realistic forces.

Experimental data:

- all atomic masses with $Z, N \geq 8$ from the Atomic Mass Evaluation (root-mean square deviation: 0.5-0.6 MeV)
  `http://www.astro.ulb.ac.be/bruslib/`
- charge radii
- symmetry energy $29 \leq J \leq 33$ MeV
- compressibility $230 \leq K_v \leq 250$ MeV

N-body calculations using realistic forces:

- equation of state of pure neutron matter
- $^1S_0$ pairing gaps in symmetric and neutron matter
- effective masses
- stability against spurious spin and spin-isospin instabilities

Brussels-Montreal Skyrme functionals

Main features of the latest functionals:

- **fit to realistic $^1S_0$ pairing gaps** in symmetric and neutron matter (BSk16-17)
  Chamel, Goriely, Pearson, Nucl.Phys.A812,72 (2008)
- **removal of spurious instabilities** in nuclear matter (BSk18)
  Chamel, Goriely, Pearson, Phys.Rev.C80,065804(2009)
- **fit to realistic neutron-matter eos** (BSk19-21)
  Goriely, Chamel, Pearson, Phys.Rev.C82,035804(2010)
- fit of the 2012 AME with different **symmetry energy** coefficients (BSk22-26)
  Goriely, Chamel, Pearson, Phys.Rev.C88,024308(2013)
- **optimal fit of the 2012 AME** - rms 0.512 MeV (BSk27*)
  Goriely, Chamel, Pearson, Phys.Rev.C88,061302(R)(2013)

Neutron-matter equation of state

The functionals BSk19, BSk20 and BSk21 were fitted to realistic neutron-matter equations of state with different of degrees of stiffness:

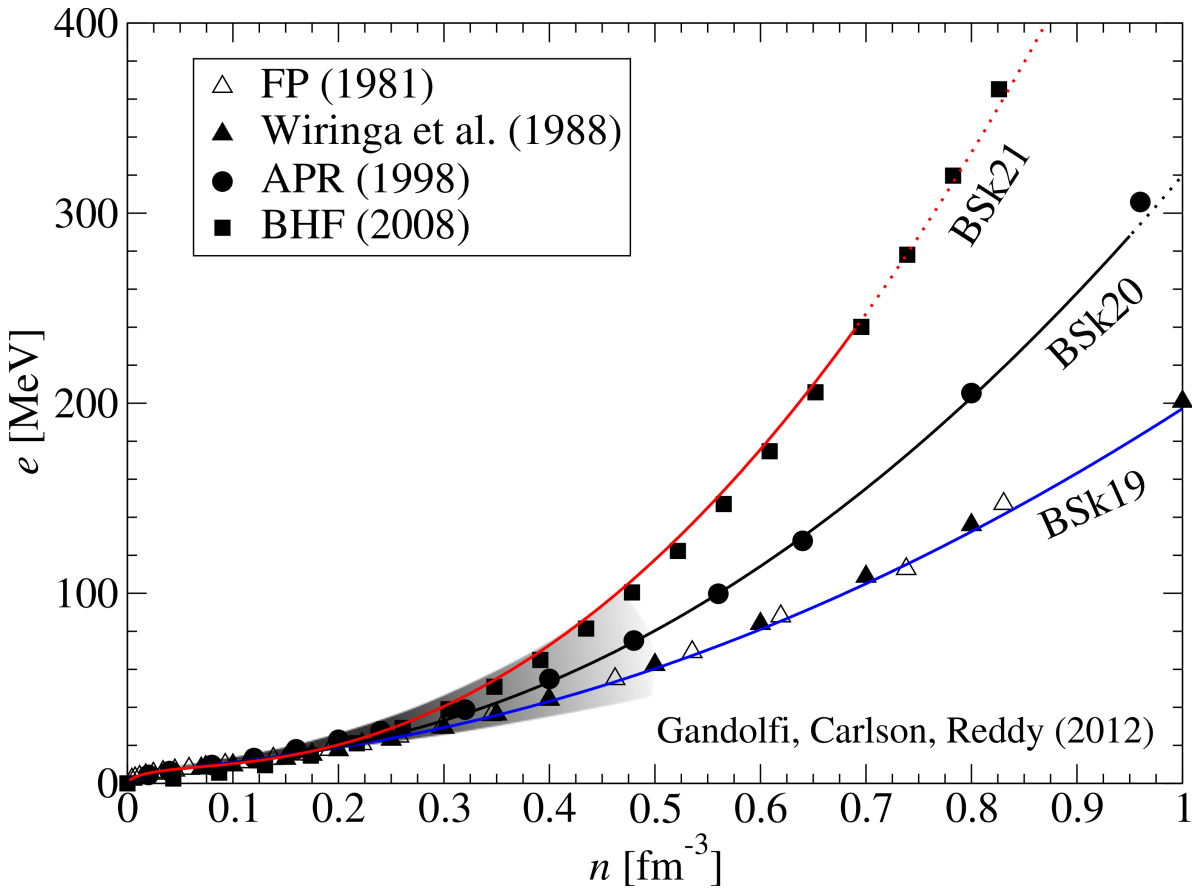

Goriely, Chamel, Pearson, Phys. Rev. C 82, 035804 (2010).

Neutron-matter equation of state at high densities

The neutron-matter equations of state obtained with these new functionals:

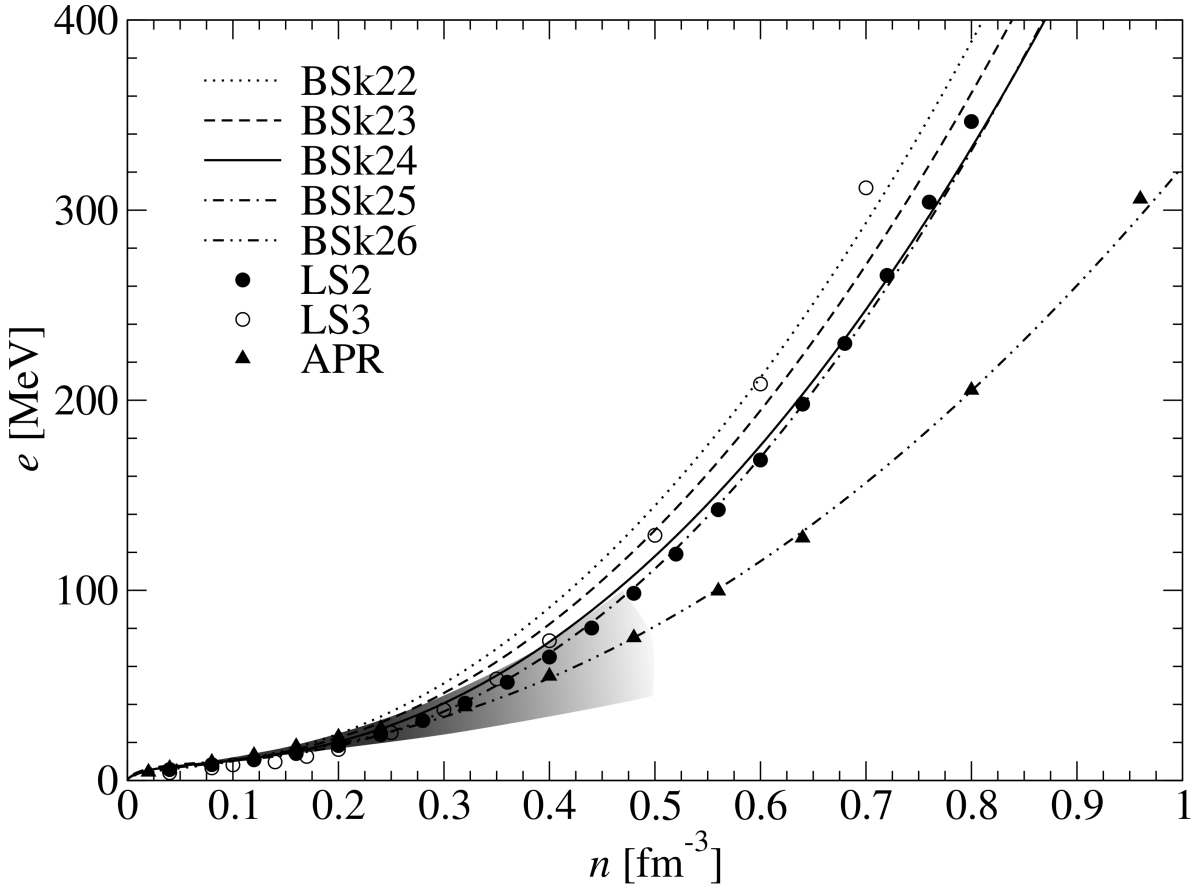

Goriely, Chamel, Pearson, Phys.Rev.C 88, 024308 (2013).

Symmetric nuclear-matter equation of state

Our functionals are also in good agreement with the constraints obtained from heavy-ion collisions:

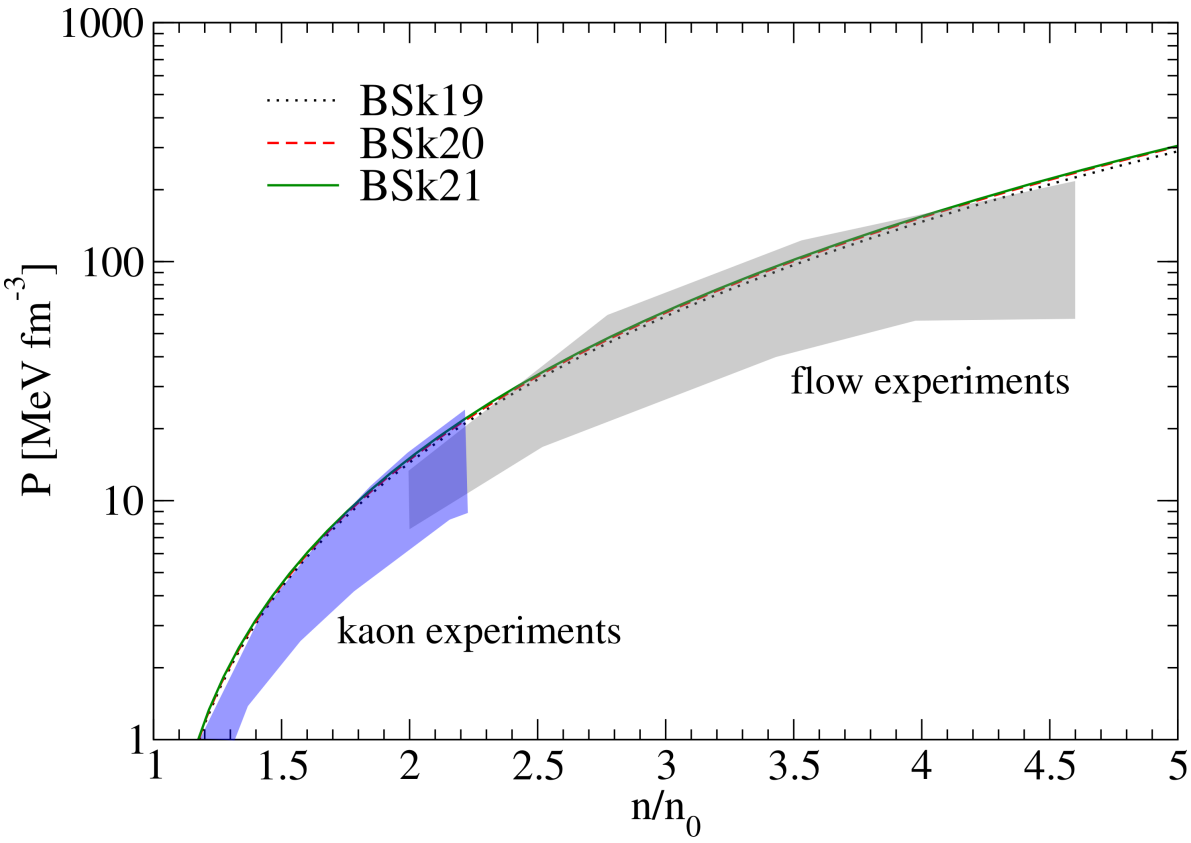

Danielewicz et al., Science 298, 1592 (2002); Lynch et al., Prog. Part. Nuc. Phys.62, 427 (2009)

Symmetry energy

The constraint obtained from our HFB atomic mass models on the symmetry energy *J* and its slope *L* (dashed line) is consistent with other experimental constraints

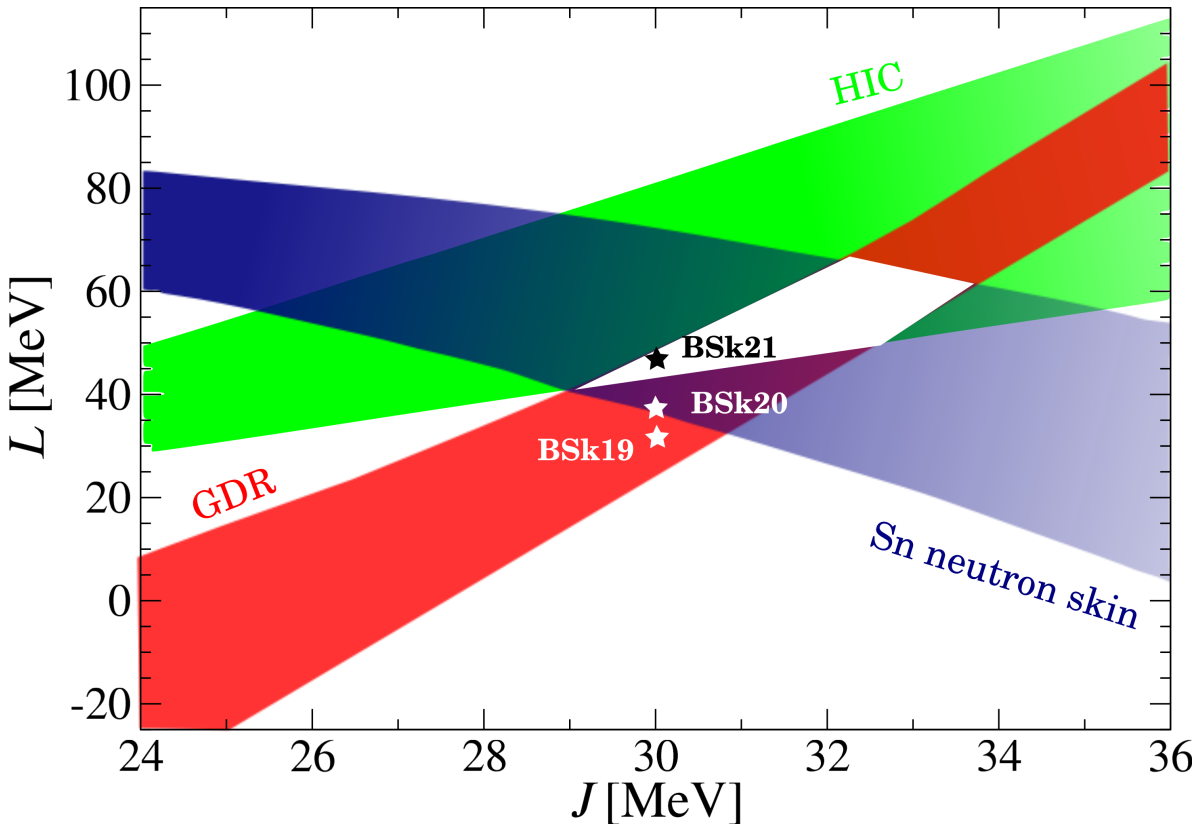

Lattimer& Steiner, EPJA50,40(2014)

Symmetry energy

The constraint obtained from about 30 different HFB atomic mass models (rms $<$ 0.84 MeV) on the symmetry energy J and its slope L (dashed line) is consistent with other experimental constraints

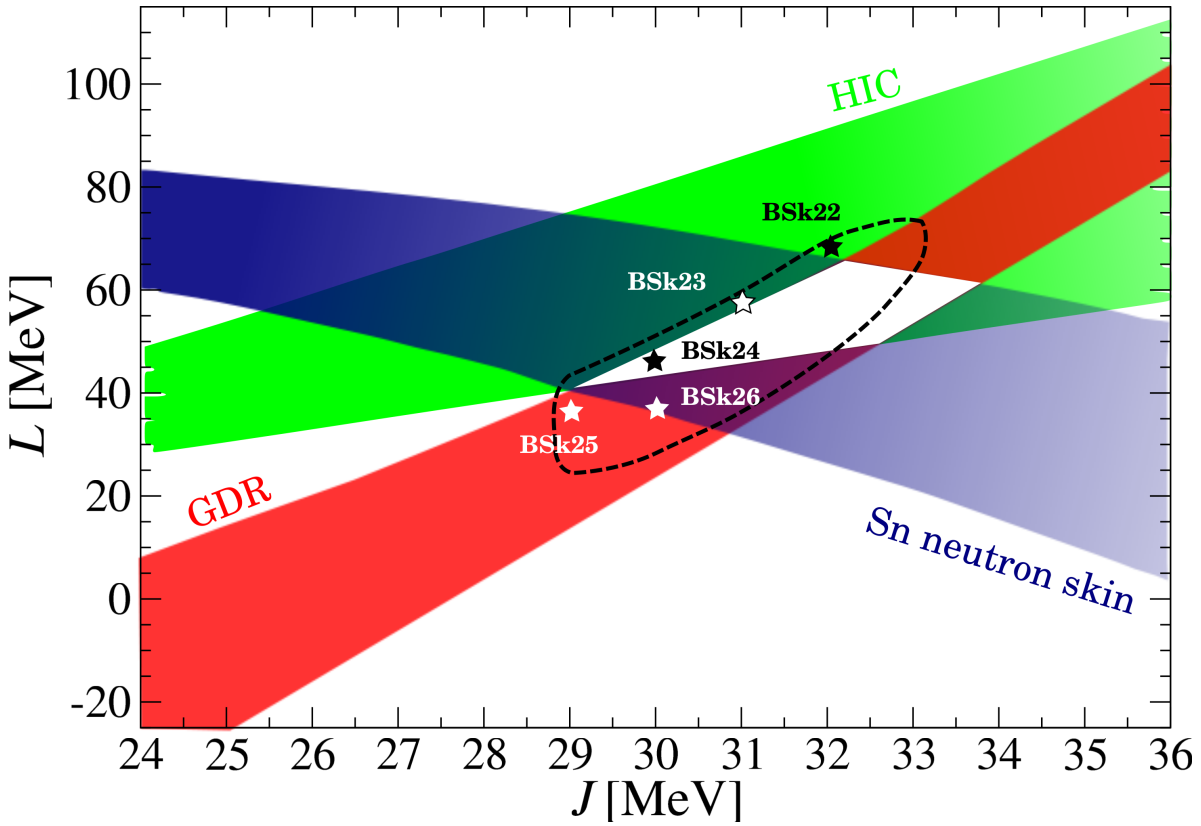

Lattimer& Steiner, EPJA50,40(2014)

Effective masses

Our functionals yield reasonable values for the nucleon effective masses consistent with giant resonances in nuclei and many-body calculations using realistic forces.

$$\frac{M}{M_q^*} = \frac{2\rho_q}{\rho}\frac{M}{M_s^*} + \left(1 - \frac{2\rho_q}{\rho}\right)\frac{M}{M_v^*}$$

	BSk19	BSk20	BSk21	EBHF
M_s^*/M	0.80	0.80	0.80	0.825
M_v^*/M	0.61	0.65	0.71	0.727

EBHF=Extended Brueckner Hartree-Fock calculation from *Cao et al.,Phys.Rev.C73,014313(2006)*.

Note that our functionals yield a correct splitting of effective masses ($M_n^* > M_p^*$ in neutron-rich matter).

Latest Brussels-Montreal Skyrme functionals

The latest functionals BSk22-26 were fitted following the same protocole but with different symmetry energy coefficients J:

	HFB-22	HFB-23	HFB-24	HFB-25	HFB-26
J [MeV]	32	31	30	29	30
NeuM	BHF	BHF	BHF	BHF	APR
$\sigma(M)$ [MeV]	0.629	0.569	0.549	0.544	0.564
$\bar{\epsilon}(M)$ [MeV]	-0.043	-0.022	-0.012	0.008	0.006
$\sigma(M_{nr})$ [MeV]	0.817	0.721	0.702	0.791	0.749
$\bar{\epsilon}(M_{nr})$ [MeV]	0.221	0.090	0.011	0.023	0.230
M_v^*/M	0.71	0.71	0.71	0.74	0.65

Goriely, Chamel, Pearson, Phys.Rev.C 88, 024308 (2013).

Structure and composition of neutron star crusts

Description of neutron star crust below neutron drip

Cold catalyzed matter hypothesis

The interior of a neutron is supposed to be in full thermodynamic equilibrium at zero temperature.

The equilibrium structure of the outer crust of a neutron star for $\rho \gtrsim 10^4$ g cm^{-3} can be determined using the BPS model:

- fully ionized atoms arranged in a bcc lattice
- homogeneous crystal at any given pressure
- uniform relativistic electron Fermi gas.

The only microscopic inputs are nuclear masses. We have made use of the experimental data (Atomic Mass Evaluation) complemented with our HFB mass tables.

Composition of the outer crust of a neutron star

The composition of the crust is completely determined by experimental nuclear masses down to about 200m for a $1.4M_{\odot}$ neutron star with a 10 km radius

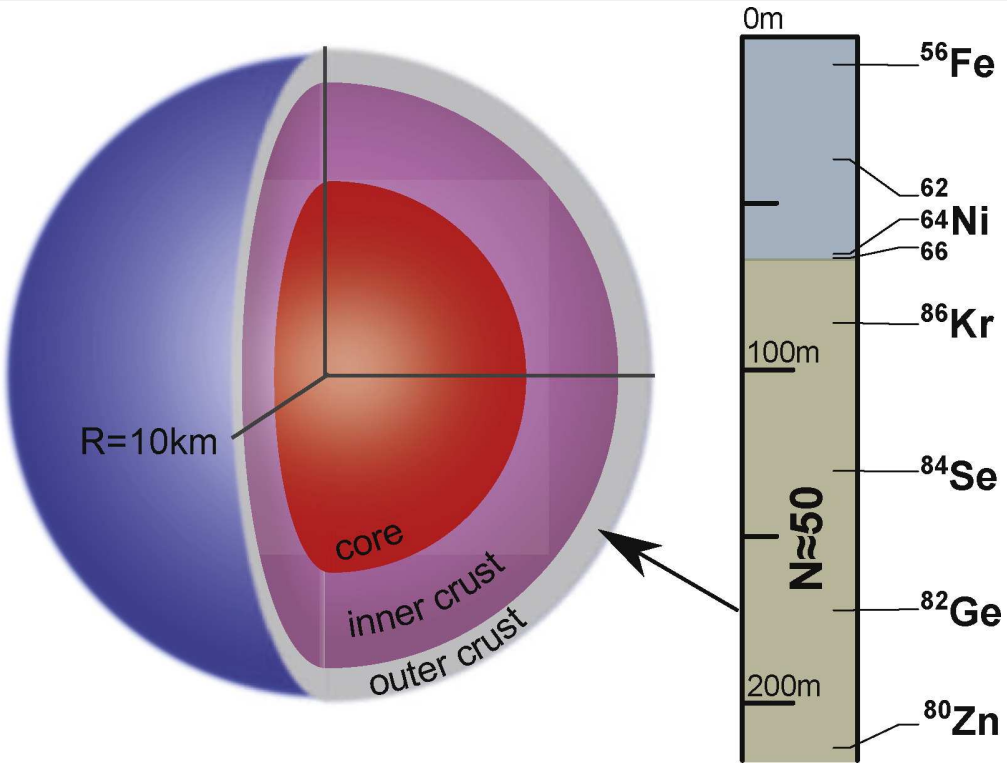

Pearson,Goriely,Chamel,Phys.Rev.C83,065810(2011); Kreim, Hempel, Lunney, Schaffner-Bielich, Int.J.M.Spec.349-350,63(2013)

Composition of the outer crust of a neutron star

Deeper in the star, the composition is model-dependent:

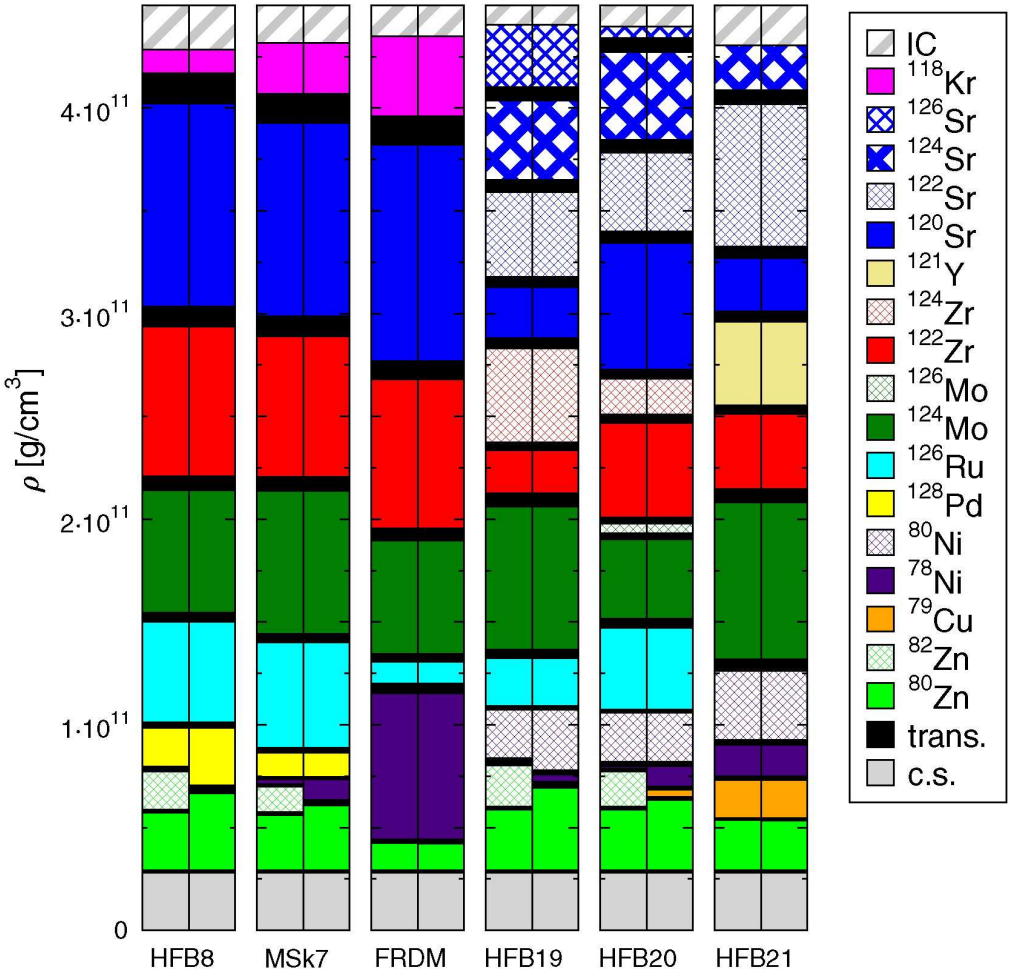

Pearson,Goriely,Chamel,Phys.Rev.C83,065810(2011); Kreim, Hempel, Lunney, Schaffner-Bielich, Int.J.M.Spec.349-350,63(2013)

Impact of a strong magnetic field on the composition of the crust?

In a strong magnetic field B (along let's say the z-axis), the **electron motion perpendicular to the field is quantized** into Landau-Rabi levels:

$$e_\nu = \sqrt{c^2 p_z^2 + m_e^2 c^4 (1 + 2\nu B_\star)}$$

where $\nu = 0, 1, ...$
$B_\star = B/B_c$
$B_c = m_e^2 c^3/\hbar e \simeq 4.4 \times 10^{13}$ G.

Only $\nu = 0$ is filled for $\rho < 2.07 \times 10^6 \left(\frac{A}{Z}\right) B_\star^{3/2}$ g cm^{-3}.

Landau quantization can impact the composition of the crust.

Composition of the outer crust of a magnetar

Sequence of nuclides for HFB-21 and $B_\star \equiv B/(4.4 \times 10^{13}\ \mathrm{G})$:

$B_\star = 0$	$B_\star = 1$	$B_\star = 10$	$B_\star = 100$	$B_\star = 1000$	$B_\star = 2000$
^{56}**Fe**	^{56}**Fe**	^{56}**Fe**	^{56}**Fe**	^{56}**Fe**	^{56}**Fe**
^{62}**Ni**	^{62}**Ni**	^{62}**Ni**	^{62}**Ni**	^{62}**Ni**	^{62}**Ni**
^{58}**Fe**	^{58}**Fe**	–	–	–	–
^{64}**Ni**	^{64}**Ni**	^{64}**Ni**	^{64}**Ni**	^{64}**Ni**	–
^{66}**Ni**	^{66}**Ni**	^{66}**Ni**	–	–	–
–	–	–	–	^{88}**Sr**	^{88}**Sr**
^{86}**Kr**	^{86}**Kr**	^{86}**Kr**	^{86}**Kr**	^{86}**Kr**	^{86}**Kr**
^{84}**Se**	^{84}**Se**	^{84}**Se**	^{84}**Se**	^{84}**Se**	^{84}**Se**
^{82}**Ge**	^{82}**Ge**	^{82}**Ge**	^{82}**Ge**	^{82}**Ge**	^{82}**Ge**
–	–	–	–	–	^{132}**Sn**
^{80}**Zn**	^{80}**Zn**	^{80}**Zn**	^{80}**Zn**	^{80}**Zn**	^{80}**Zn**
–	–	–	–	–	^{130}**Cd**
–	–	–	–	–	^{128}Pd
–	–	–	–	–	^{126}Ru
^{79}Cu	^{79}Cu	^{79}Cu	^{79}Cu	^{79}Cu	–
^{78}Ni	^{78}Ni	^{78}Ni	^{78}Ni	^{78}Ni	–
^{80}Ni	^{80}Ni	^{80}Ni	^{80}Ni	^{80}Ni	–
^{124}Mo	^{124}Mo	^{124}Mo	^{124}Mo	^{124}Mo	^{124}Mo
^{122}Zr	^{122}Zr	^{122}Zr	^{122}Zr	^{122}Zr	^{122}Zr
^{121}Y	^{121}Y	^{121}Y	^{121}Y	^{121}Y	^{121}Y
^{120}Sr	^{120}Sr	^{120}Sr	^{120}Sr	^{120}Sr	^{120}Sr
^{122}Sr	^{122}Sr	^{122}Sr	^{122}Sr	^{122}Sr	^{122}Sr
^{124}Sr	^{124}Sr	^{124}Sr	^{124}Sr	^{124}Sr	^{124}Sr

Chamel et al.,Phys.Rev.C86, 055804(2012).

Equation of state of the outer crust of magnetars

Matter in a magnetar is much more incompressible and less neutron-rich than in a neutron star.

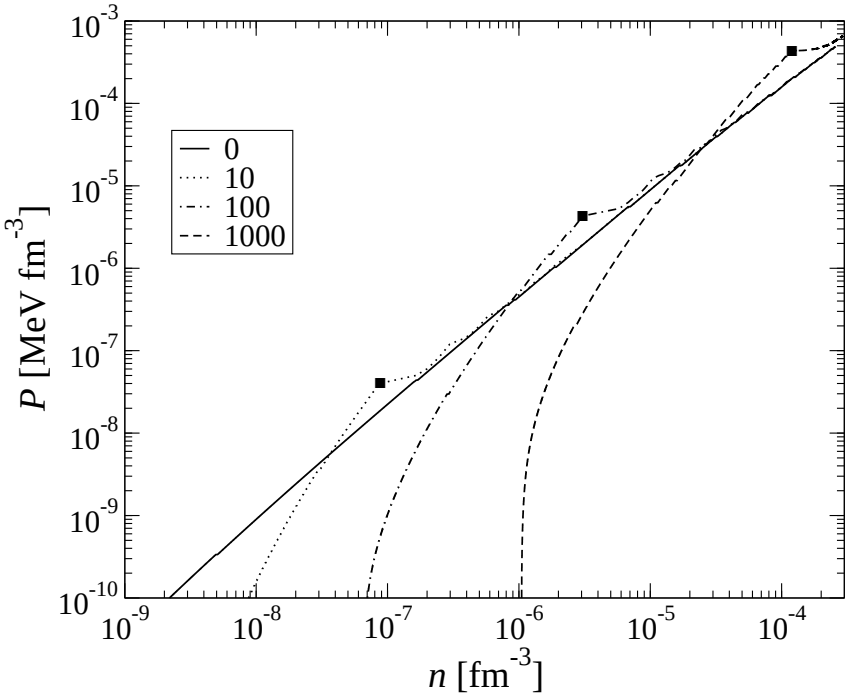

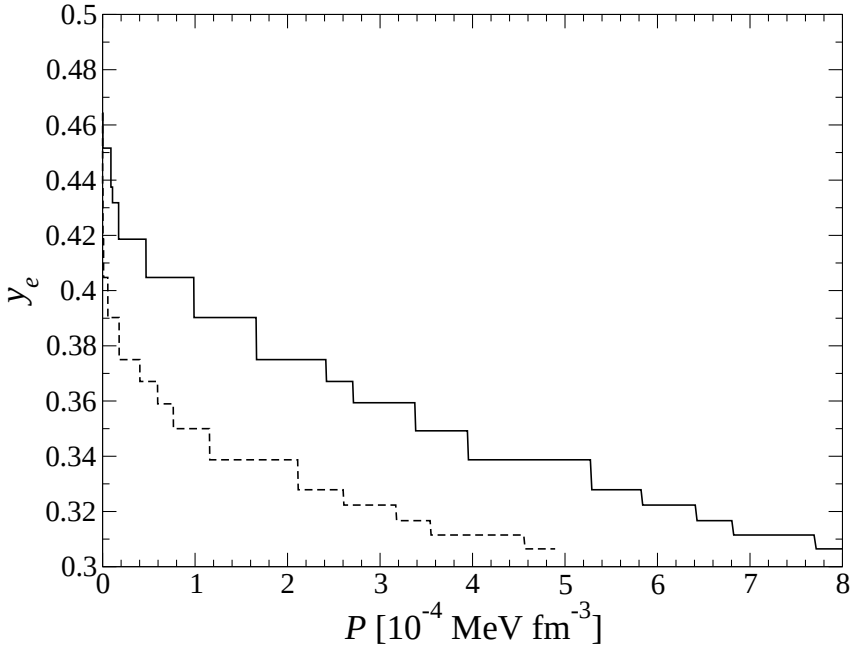

$$P \approx P_0 \left(\frac{n}{n_s} - 1 \right)^2$$

$$y_e \approx \frac{1}{2} \left(1 - \sqrt{\frac{\pi^2 \lambda_e^3 m_e c^2 P}{4 B_\star J^2}} \right)$$

Neutron drip transition in magnetars

The neutron drip pressure is found to increase with B whereas the composition of matter remains the same:

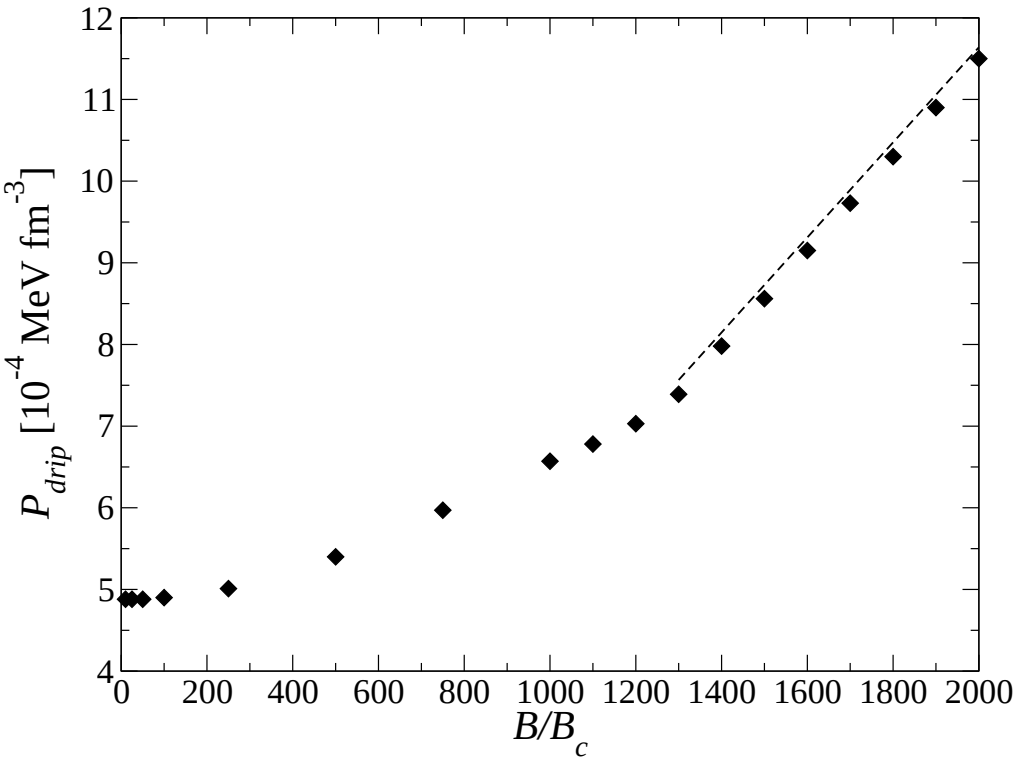

In the strongly quantizing regime, $P_{\rm drip} = \dfrac{m_e c^2}{\lambda_e^3} \dfrac{(\gamma_e^{\rm drip})^2}{4\pi^2} B_\star$

Description of neutron star crust beyond neutron drip

We have determined the equilibrium structure of the inner crust of a neutron star for $\rho \gtrsim 4 \times 10^{11}$g cm^{-3} using the Extended Thomas-Fermi+Strutinsky Integral method (ETFSI):

- spherical neutron-proton clusters coexisting with a neutron liquid using parametrized density distributions (Wigner-Seitz approximation for the Coulomb energy),
- proton shell effects added perturbatively,
- uniform relativistic electron gas.

Pearson,Chamel,Goriely,Ducoin,Phys.Rev.C85,065803(2012).

Advantages of ETFSI method

- very fast approximation to the full Hartree-Fock method
- avoids the difficulties related to boundary conditions *Chamel et al.,Phys.Rev.C75(2007),055806.*

Structure of the inner crust of a neutron star (I) nucleon distributions

With increasing density, the clusters keep essentially the same size but become more and more dilute:

Crust-core transition properties

	$\bar{n}_{cc}$ (fm^{-3})	P_{cc} (MeV fm^{-3})
BSk19	0.0885	0.428
BSk20	0.0854	0.365
BSk21	0.0809	0.268
SLy4	0.0798	0.361

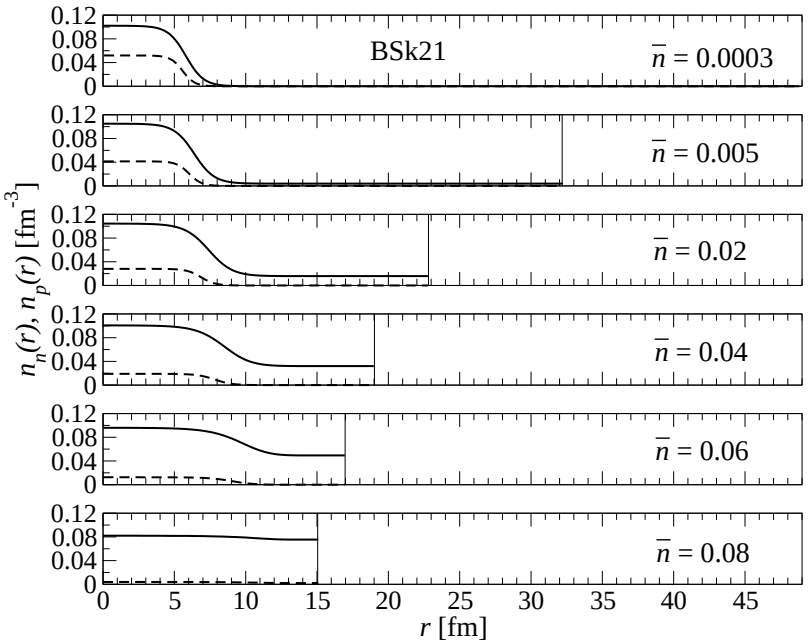

Open issues: pastas?

The crust-core transition is very smooth: the crust dissolves continuously into a uniform mixture of nucleons and electrons.

Structure of the inner crust of a neutron star (II) composition

With SLy4, BSk19, BSk20 and BSk21, only $Z = 40$ is found.

Comparison of inner- and outer-crust codes at drip point; results for latter code in parentheses. e is the internal energy per nucleon, and P the pressure.

	$\bar{n}_{\rm drip}$ (fm^{-3})	Z	N	e (MeV)	P (10^{-4} MeV fm^{-3})
BSk19	2.63×10^{-4}	40 (38)	96 (88)	-1.79 (-1.87)	5.1 (4.9)
BSk20	2.63×10^{-4}	40 (38)	95 (88)	-1.79 (-1.87)	5.1 (4.9)
BSk21	2.57×10^{-4}	40 (38)	94 (86)	-1.82 (-1.90)	5.0 (4.9)
SLy4	2.46×10^{-4}	40 (38)	93 (82)	-1.79 (-1.96)	4.7 (4.8)

The few % discrepancies can be attributed to

- the neglect of pairing,
- the neglect of neutron shell effects,
- the parametrized density distributions,
- the neglect of rotational and vibrational corrections.

Structure of the inner crust of a neutron star (II) composition

- The ordinary nuclear shell structure seems to be preserved apart from $Z = 40$ (quenched spin-orbit?).
- The energy differences between different configurations become very small as the density increases

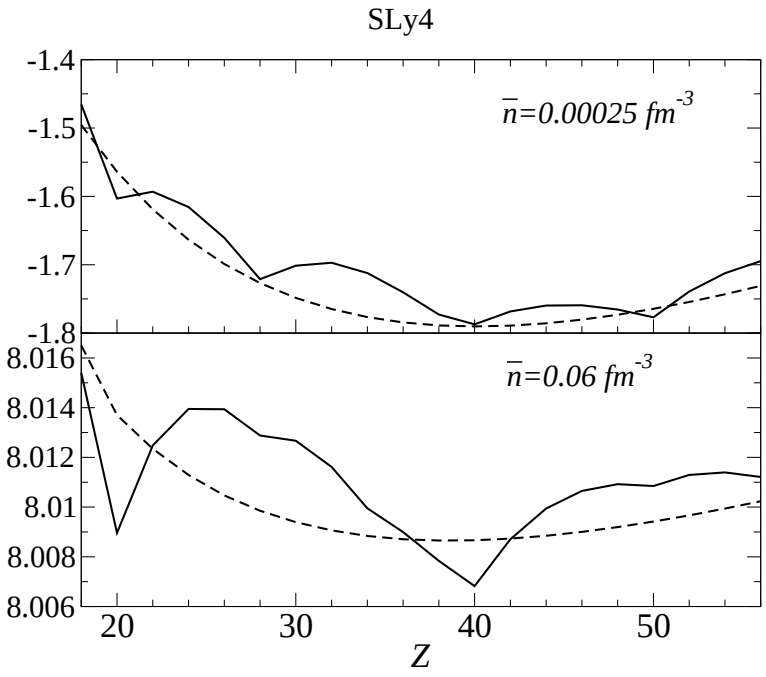

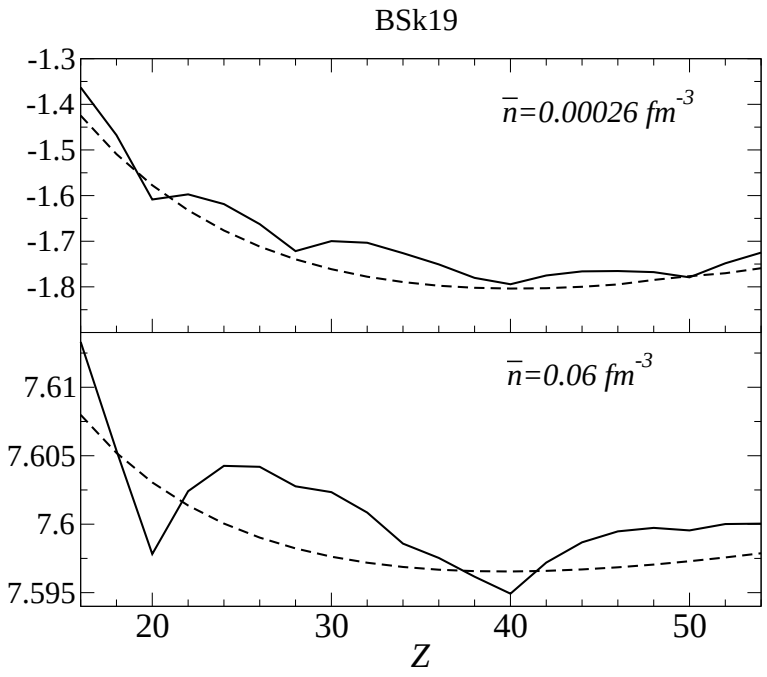

Structure of the inner crust of a neutron star (III) composition

Impact of proton pairing (BCS approximation) with BSk21

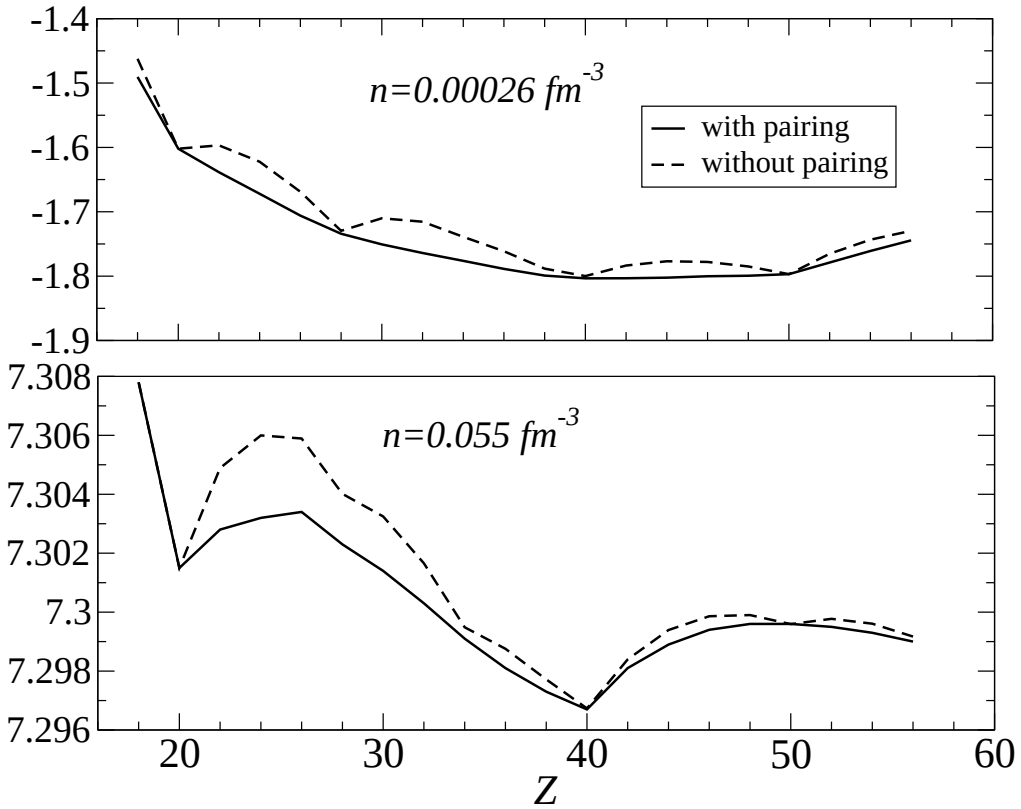

Impact of neutron pairing on the crust structure?

Pearson,Chamel,Pastore,Goriely,submitted.

In a real neutron star, a large range of values of Z is expected.

Unified equations of state of neutron stars

The same functionals used in the crust can be also used to compute the equation of state of the core, assuming it is made of n, p, e^- and μ^-.

Tables of the full equations of state:

`http://vizier.cfa.harvard.edu/viz-bin/VizieR?-source=J/A+A/559/A128`

Fantina, Chamel, Pearson, Goriely, A&A 559, A128 (2013)

Analytical representations of the full equations of state (fortran subroutines):

`http://www.ioffe.ru/astro/NSG/BSk/`

Potekhin, Fantina, Chamel, Pearson, Goriely, A&A 560, A48 (2013)

EoSs for the latest BSk functionals will appear soon.

Pearson, Chamel, Fantina, Goriely, Eur. Phys. J. A 50, 43 (2014)

Adiabatic index

Realistic equations of state can hardly be parametrized by polytropes:

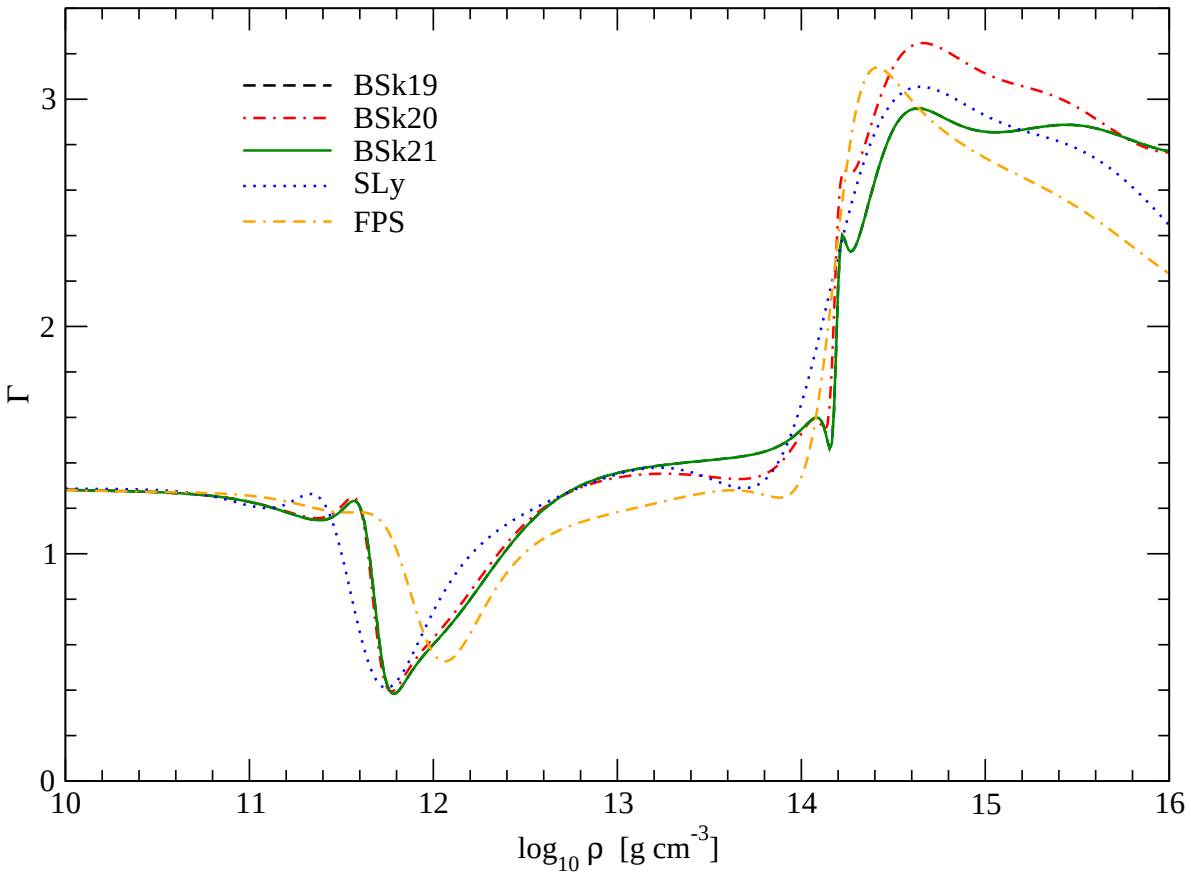

Potekhin, Fantina, Chamel, Pearson, Goriely, A&A 560, A48 (2013)

Neutron star structure

With these unified equations of state, we have computed the global structure of neutron stars by solving the TOV equations:

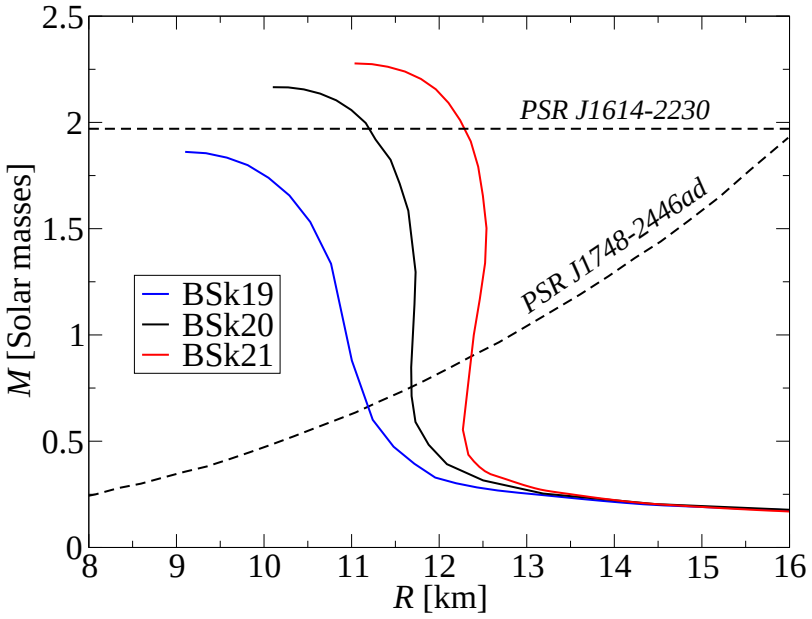

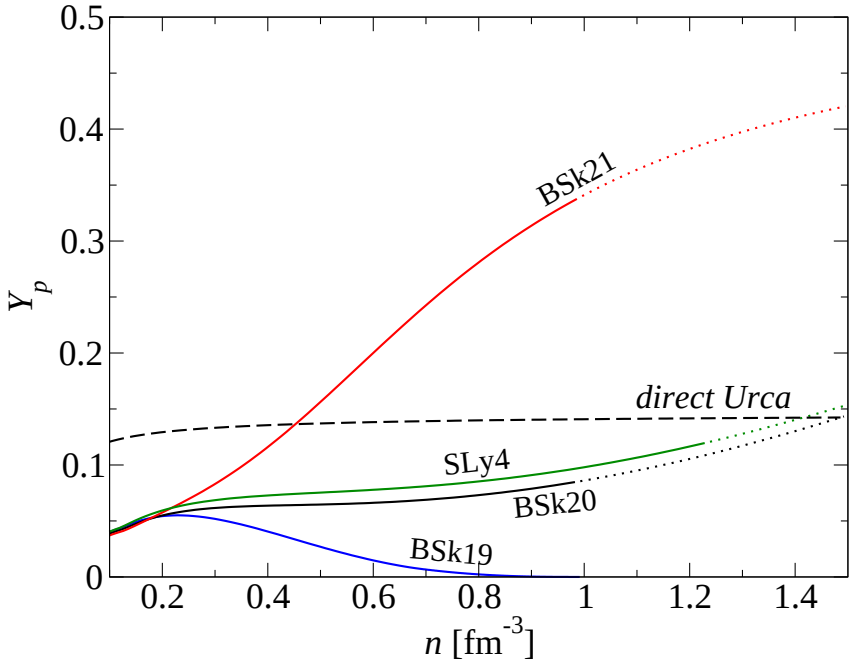

Chamel, Fantina, Pearson, Goriely,Phys.Rev.C84,062802(R)(2011).

Superfluidity in neutron-star crusts

Superfluidity in neutron-star crusts with the Wigner-Seitz approximation

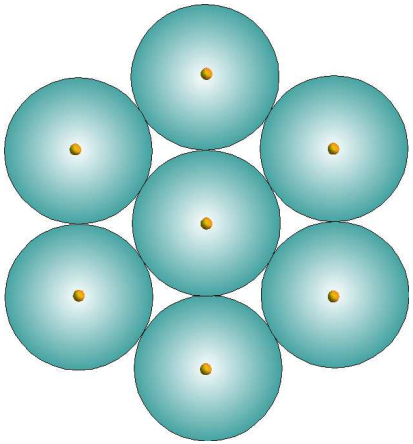

Superfluidity has been already studied with the HFB method using the Wigner-Seitz approximation. However, this approach breaks down in the deep region of the crust
Chamel et al., Phys.Rev.C75(2007)055806.

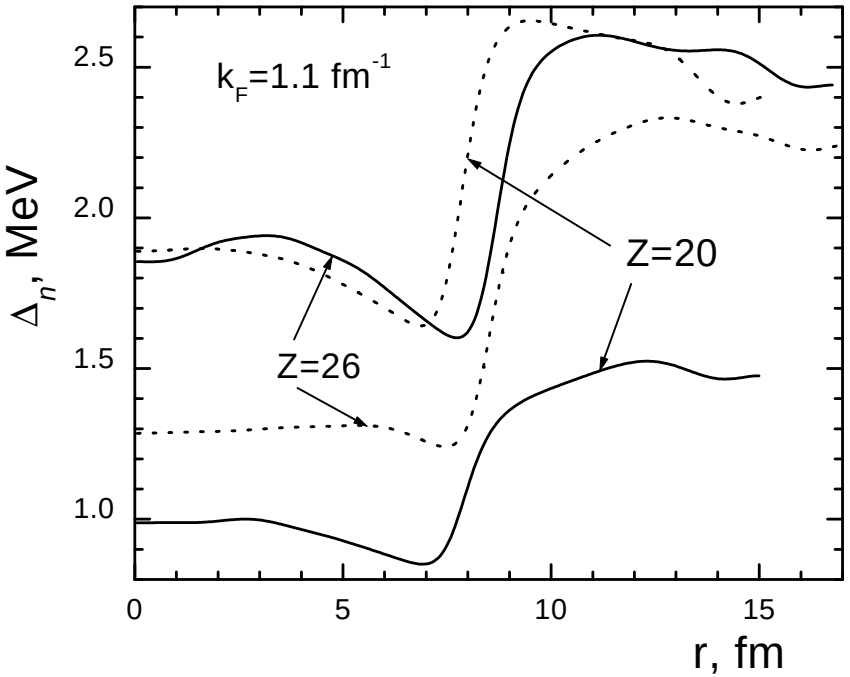

Spurious shell effects $\propto 1/R^2$ can be very large at the crust bottom and are enhanced by the self-consistency.
Baldo et al., EPJA32,97(2007).

Pairing in the deep region of the inner crust

These limitations can be overcome by using the band theory.

At high densities, the HFB equations can be approximated by the **anisotropic multi-band BCS equations**:

$$\Delta_{\alpha\boldsymbol{k}} = -\frac{1}{2}\sum_{\beta}\int \frac{\mathrm{d}^3\boldsymbol{k'}}{(2\pi)^3}\bar{v}^{\mathrm{pair}}_{\alpha\boldsymbol{k}\,\alpha-\boldsymbol{k}\,\beta\boldsymbol{k'}\,\beta-\boldsymbol{k'}}\frac{\Delta_{\beta\boldsymbol{k'}}}{E_{\beta\boldsymbol{k'}}}\tanh\frac{E_{\beta\boldsymbol{k'}}}{2k_{\mathrm{B}}T}$$

$$\bar{v}^{\mathrm{pair}}_{\alpha\boldsymbol{k}\,\alpha-\boldsymbol{k}\,\beta\boldsymbol{k'}\,\beta-\boldsymbol{k'}} = \int \mathrm{d}^3r\, v^{\pi}[\rho_n(\boldsymbol{r}),\rho_p(\boldsymbol{r})]\,|\varphi_{\alpha\boldsymbol{k}}(\boldsymbol{r})|^2|\varphi_{\beta\boldsymbol{k'}}(\boldsymbol{r})|^2$$

$$E_{\alpha\boldsymbol{k}} = \sqrt{(\varepsilon_{\alpha\boldsymbol{k}}-\mu)^2+\Delta^2_{\alpha\boldsymbol{k}}}$$

$\varepsilon_{\alpha\boldsymbol{k}}$, μ and $\varphi_{\alpha\boldsymbol{k}}(\boldsymbol{r})$ are obtained from band structure calculations using the ETFSI mean fields

Chamel et al., Phys.Rev.C81,045804 (2010).

Neutron pairing gaps

Results obtained for BSk16
n_n^f is the density of unbound neutrons
$\Delta_{\rm u}$ is the gap in neutron matter at density n_n^f
$\bar{\Delta}_{\rm u}$ is the gap in neutron matter at density n_n

$\bar{n}$ [fm^{-3}]	Z	A	n_n^f [fm^{-3}]	$\Delta_{\rm F}$ [MeV]	$\Delta_{\rm u}$ [MeV]	$\bar{\Delta}_{\rm u}$ [MeV]
0.07	40	1218	0.060	1.44	1.79	1.43
0.065	40	1264	0.056	1.65	1.99	1.65
0.06	40	1260	0.051	1.86	2.20	1.87
0.055	40	1254	0.047	2.08	2.40	2.10
0.05	40	1264	0.043	2.29	2.59	2.33

- $\Delta_{\alpha \boldsymbol{k}}(T)/\Delta_{\alpha \boldsymbol{k}}(0)$ is a universal function of T
- The critical temperature is approximately given by the usual BCS relation $T_{\rm c} \simeq 0.567 \Delta_{\rm F}$
- the nuclear clusters lower the gap by $10-20\%$

Pairing field and local density approximation

The effects of inhomogeneities on neutron superfluidity can be directly seen in the pairing field

$$\Delta_n(\boldsymbol{r}) = -\frac{1}{2} v^{\pi n}[\rho_n(\boldsymbol{r}), \rho_p(\boldsymbol{r})] \sum_{\alpha} \int \frac{\mathrm{d}^3\boldsymbol{k}}{(2\pi)^3} |\varphi_{\alpha\boldsymbol{k}}(\boldsymbol{r})|^2 \frac{\Delta_{\alpha\boldsymbol{k}}}{E_{\alpha\boldsymbol{k}}}$$

Neutron pairing field for $\bar{n} = 0.06$ fm^{-3} at $T = 0$:

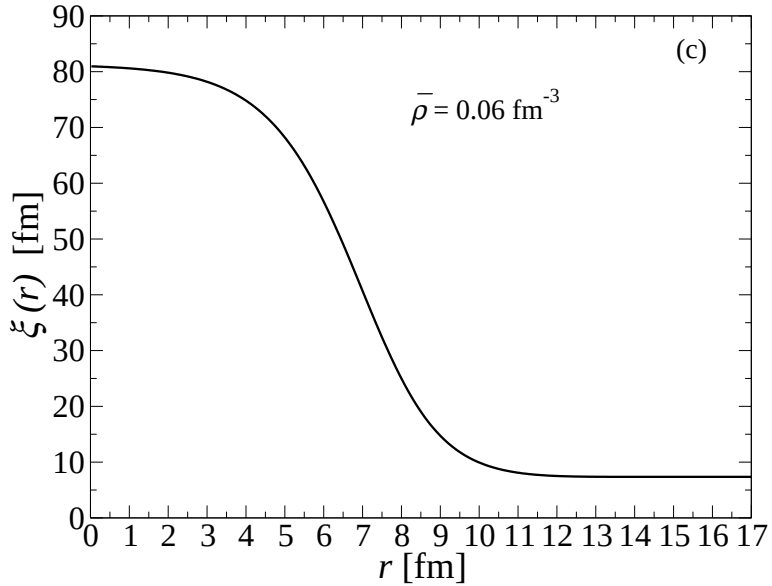

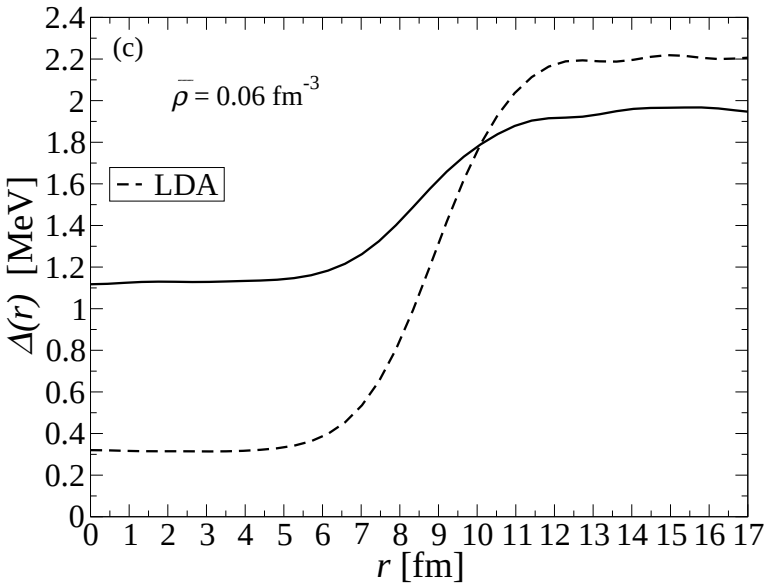

The superfluid permeates the clusters due to proximity effects.

Pairing in the shallow region of the inner crust

The dilute superfluid does not follow the usual BCS behavior.

HFB calculations in the W-S approximation with SLy4:

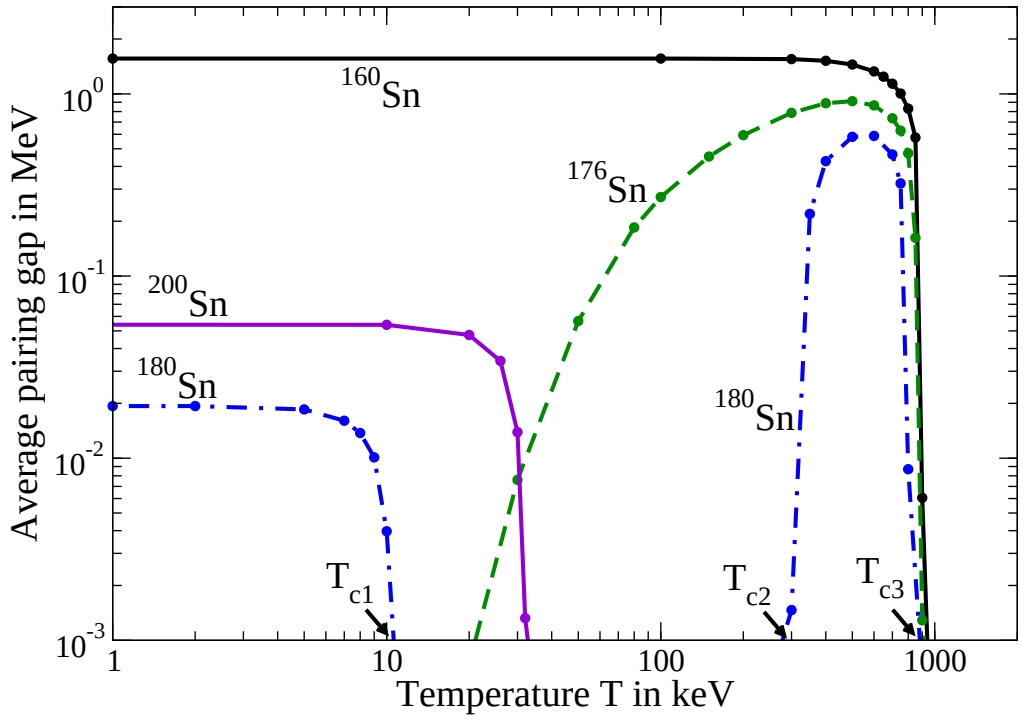

Margueron& Khan, Phys.Rev.C86,065801(2012).

Pairing in the shallow region of the inner crust

Similar results are found from 3D HFB calculations with Bloch boundary conditions.

Preliminary results for ^{185}Sn at $\bar{n} = 0.0003$ fm^{-3} with BSk16:

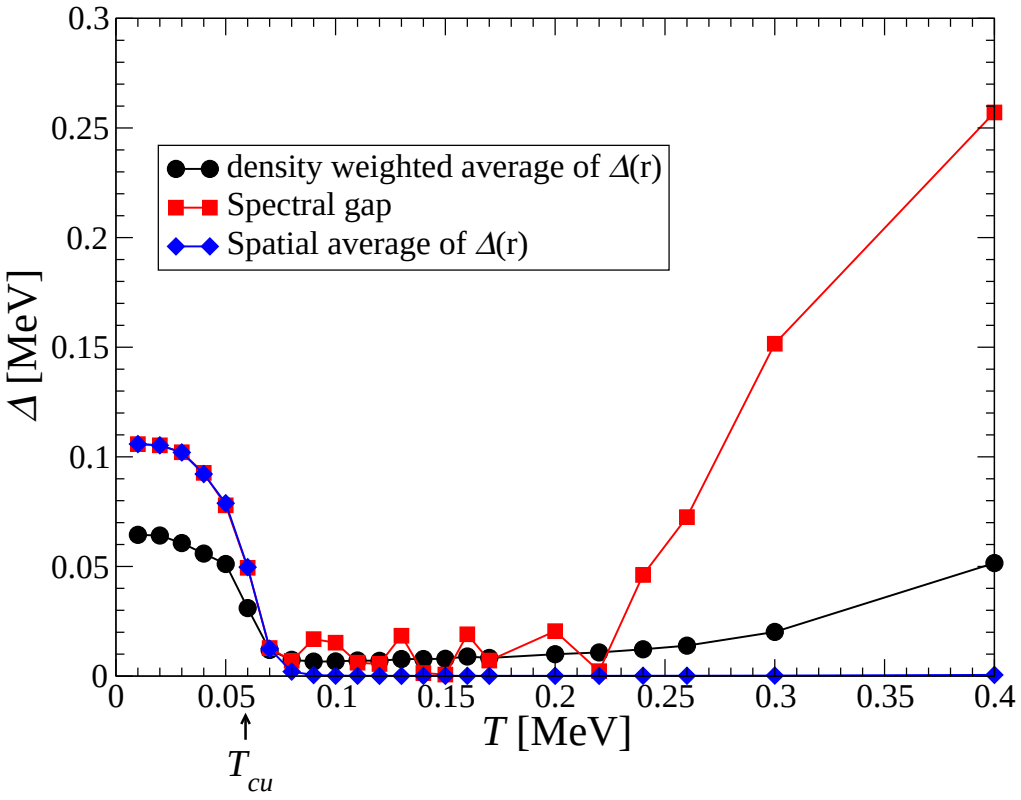

Entrainment in neutron-star crusts

Despite the absence of viscous drag, the crust can still resist the flow of the superfluid due to non-local and non-dissipative entrainment effects.

Carter, Chamel & Haensel, Nucl.Phys.A748,675(2005).

What is entrainment?

A neutron with wavevector $\boldsymbol{k}$ can be **coherently scattered** by the lattice if $d \sin\theta = N\pi/k$, where $N = 0, 1, 2, ...$ (Bragg's law).

In this case, it does not propagate in the crystal: it is therefore entrained!

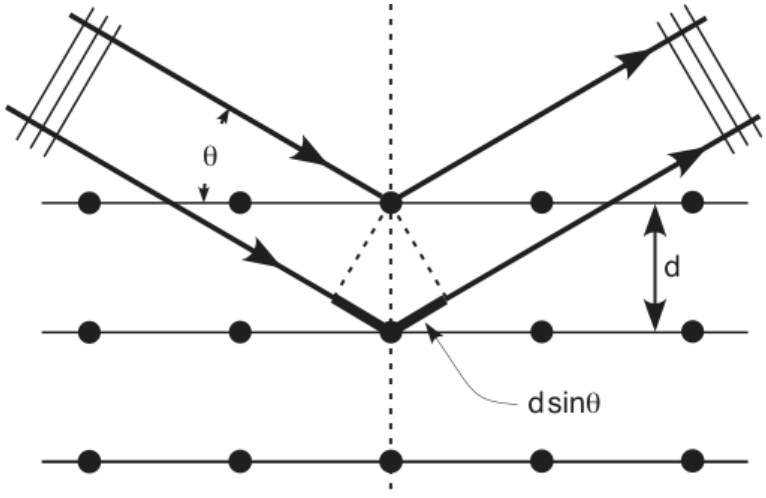

Neutron diffraction

For decades, neutron diffraction experiments have been routinely performed to explore the structure of materials.

The main difference in neutron-star crusts is that neutrons are highly degenerate

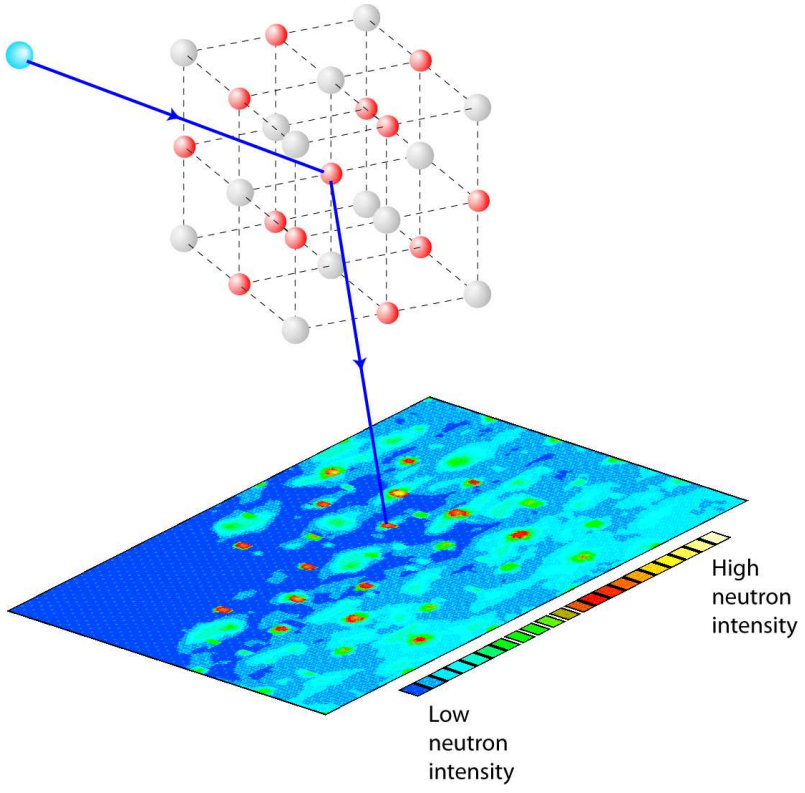

A neutron can be coherently scattered if $k > \pi/d$. In neutron stars, neutrons have momenta up to k_{F}. Typically $k_{\mathrm{F}} > \pi/d$ in all regions of the inner crust but the shallowest. Therefore, Bragg scattering should be taken into account!

How “free” are neutrons in neutron-star crusts?

$\bar{n}$ (fm^{-3})	n_n^f/n_n (%)	n_n^c/n_n^f (%)
0.0003	20.0	82.6
0.001	68.6	27.3
0.005	86.4	17.5
0.01	88.9	15.5
0.02	90.3	7.37
0.03	91.4	7.33
0.04	88.8	10.6
0.05	91.4	30.0
0.06	91.5	45.9

$\bar{n}$ is the average baryon density
n_n is the total neutron density
n_n^f is the “free” neutron density
n_n^c is the “conduction” neutron density

Open issues: pastas? quantum and thermal fluctuations? impurities and defects?

Most neutrons are actually entrained by the crust. Entrainment can impact our understanding of various dynamical phenomena.
Chamel,Phys.Rev.C85,035801(2012).

Vela pulsar glitches and crustal entrainment

Vela pulsar glitches are usually interpreted as **sudden tranfers of angular momentum between the crustal superfluid and the rest of star**.

However this superfluid is also entrained ! Its angular momentum can thus be written as

$$J_s = I_{ss}\Omega_s + (I_s - I_{ss})\Omega_c$$

(Ω_s and Ω_c being the angular velocities of the superfluid and the “crust”), leading to the following constraint:

$$\frac{(I_s)^2}{I_{ss}I} \geq A_g \frac{\Omega}{|\dot{\Omega}|}, \qquad A_g = \frac{1}{t}\sum_i \frac{\Delta\Omega_i}{\Omega}$$

Chamel&Carter,MNRAS368,796(2006)

Pulsar glitch constraint

Since 1969, 17 glitches have been regularly detected. The latest one occurred in August 2010.

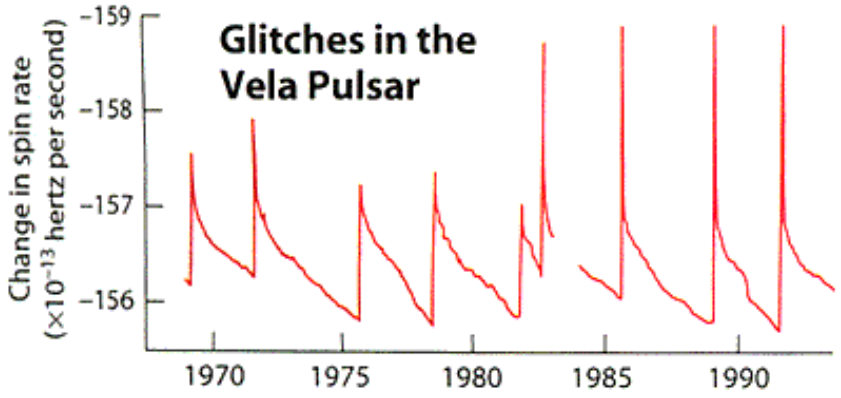

Cumulated glitch amplitude

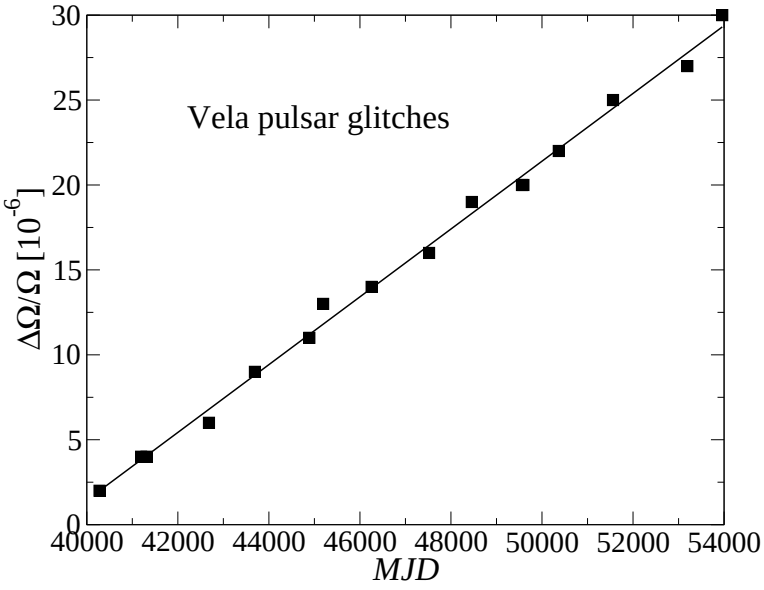

A linear fit of $\frac{\Delta\Omega}{\Omega}$ vs t yields

$A_g \simeq 2.25 \times 10^{-14}\ s^{-1}$

$$\frac{(I_s)^2}{I_{ss} I} \geq 1.6\%$$

Moments of inertia

The ratio $(I_s)^2/I_{ss}I$ depends on the internal structure of the star:

$$\frac{(I_s)^2}{II_{ss}} = \frac{I_{\rm crust}}{I_{ss}} \left(\frac{I_s}{I_{\rm crust}}\right)^2 \frac{I_{\rm crust}}{I} \,.$$

$I_{ss}/I_{\rm crust}$ and $I_s/I_{\rm crust}$ depend only on the crust physics:

$$\frac{I_{ss}}{I_{\rm crust}} \approx \frac{1}{P_{cc}} \int_{P_{\rm drip}}^{P_{cc}} \frac{n_n^{\rm f}(P)^2}{\bar{n}(P) n_n^{\rm c}(P)} \, {\rm d}P \,, \qquad \frac{I_s}{I_{\rm crust}} \approx \frac{1}{P_{\rm core}} \int_{P_{\rm drip}}^{P_{cc}} \frac{n_n^{\rm f}(P)}{\bar{n}(P)} \, {\rm d}P \,.$$

Using our crust model, we find $I_{ss} \simeq 4.6 I_{\rm crust}$ and $I_s \simeq 0.89 I_{\rm crust}$ leading to $(I_s)^2/I_{ss} \simeq 0.17 I_{\rm crust}$.

The pulsar glitch constraint thus becomes $\frac{I_{\rm crust}}{I} \geq 9.4\%$.

The ratio $I_{\rm crust}/I$ depends on the global structure of the star (M, R) and the crust-core transition (n_{cc}, P_{cc}).

Pulsar glitch constraint

Shaded areas are excluded if Vela pulsar glitches originate in the crust (Lattimer&Prakash interpolation formula was used):

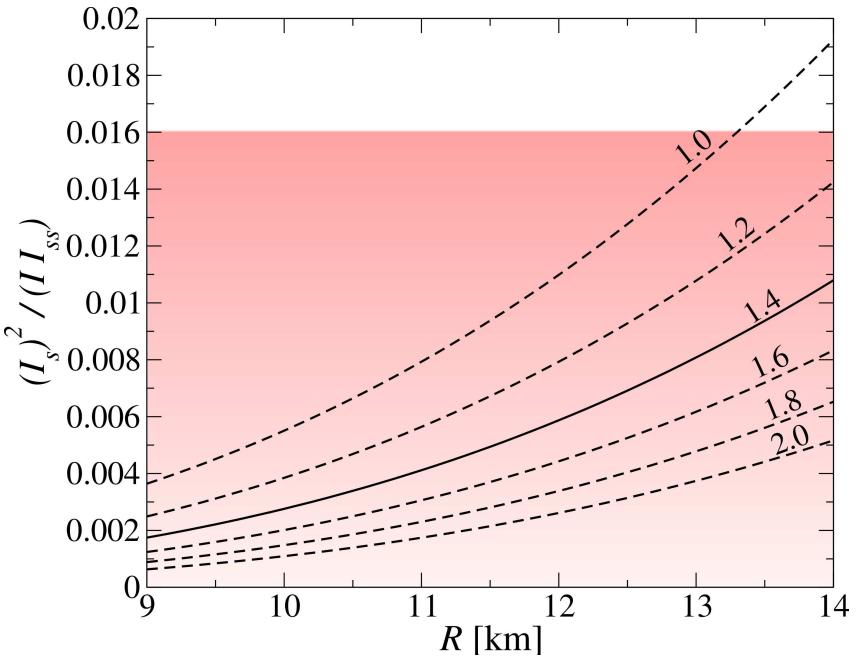

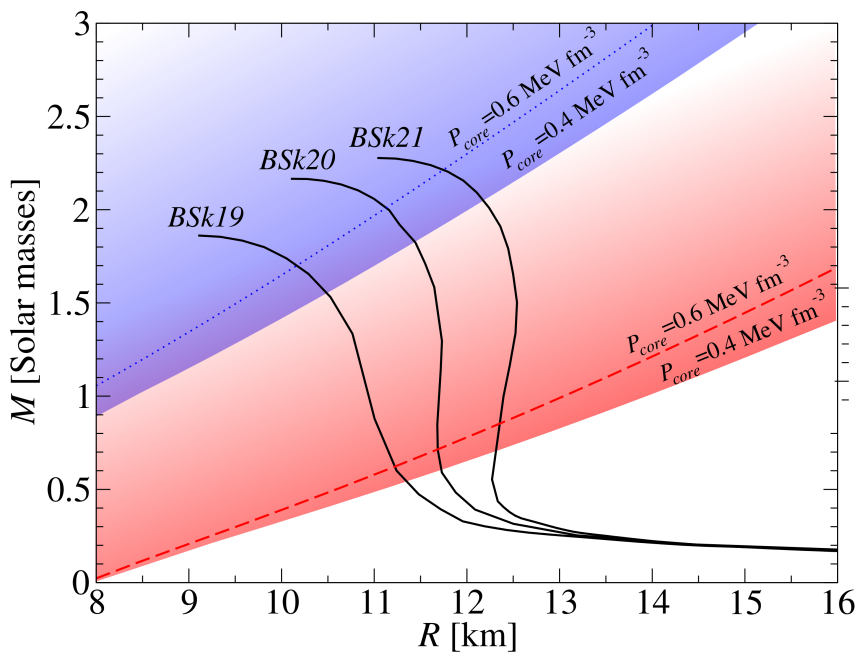

The inferred mass of Vela is unrealistically low $M < M_{\odot}$.

Due to entrainment, the superfluid in the crust does not carry enough angular momentum to explain large glitches.

Andersson et al.PRL 109, 241103; Chamel, PRL 110, 011101.

Collective excitations and thermal properties

Entrainment and collective excitations

Entrainment impacts low-energy collective excitations:

- it makes clusters heavier,
- it mixes longitudinal excitations.

Chamel,Page,Reddy,Phys.Rev.C87,035803(2013).

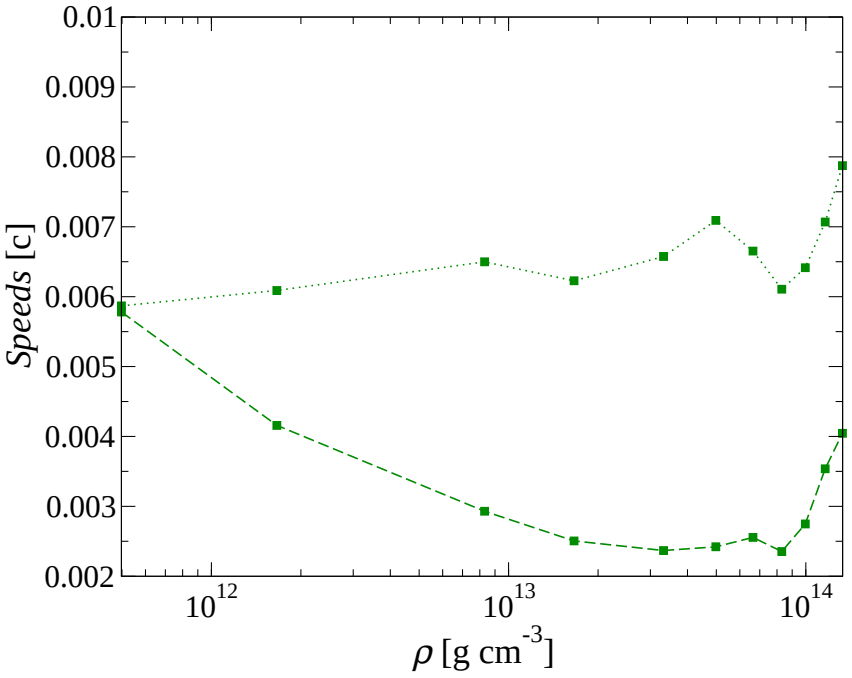

Transverse lattice phonon speeds with (dashed line) and without (dotted line) entrainment.

Entrainment and collective excitations

Entrainment impacts low-energy collective excitations:

- it makes clusters heavier,
- it mixes longitudinal excitations.

Chamel,Page,Reddy,Phys.Rev.C87,035803(2013).

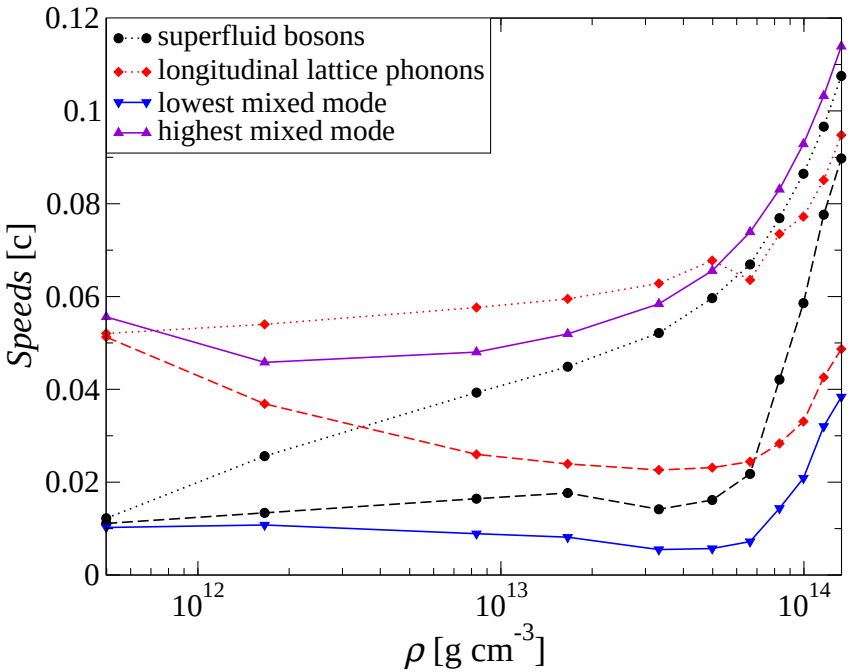

Longitudinal phonon speeds with (dashed line) and without (dotted line) entrainment but no mixing. Solids lines include entrainment and mixing.

Entrainment and thermal properties

The contribution of collective excitations to the specific heat at low T varies like $(k_{\rm B}T/\hbar v)^3$. Since entrainment reduces v, the specific heat is enhanced.

Contributions to the crustal specific heat at $T = 10^7$ K :

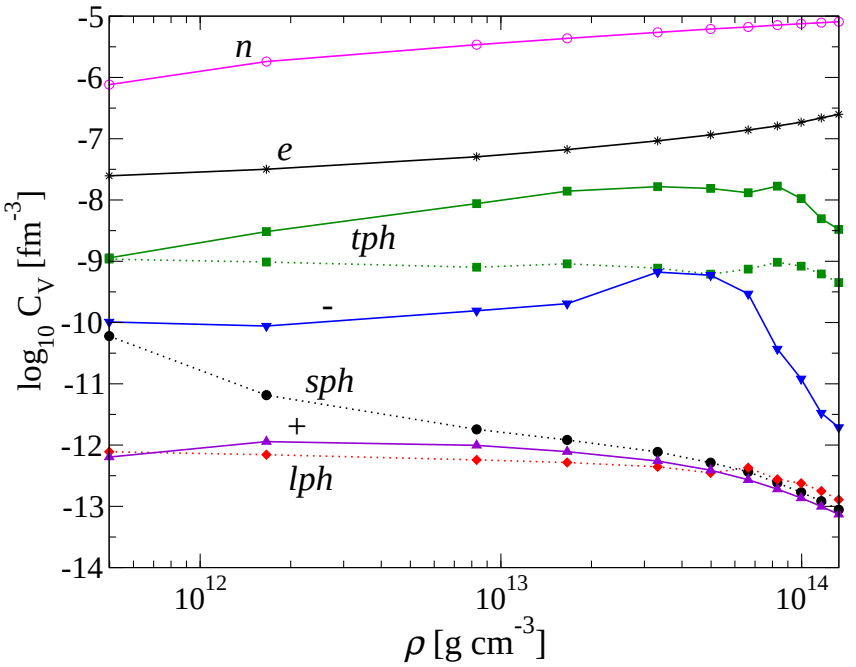

n normal neutrons
e electrons
tph transverse lattice phonons
lph longitudinal lattice phonons (without mixing)
sph superfluid phonons (without mixing)
$\pm$ longitudinal mixed modes

Entrainment and thermal properties

The contribution of collective excitations to the specific heat at low T varies like $(k_{\rm B}T/\hbar v)^3$. Since entrainment reduces v, the specific heat is enhanced.

Contributions to the crustal specific heat at $T = 10^8$ K :

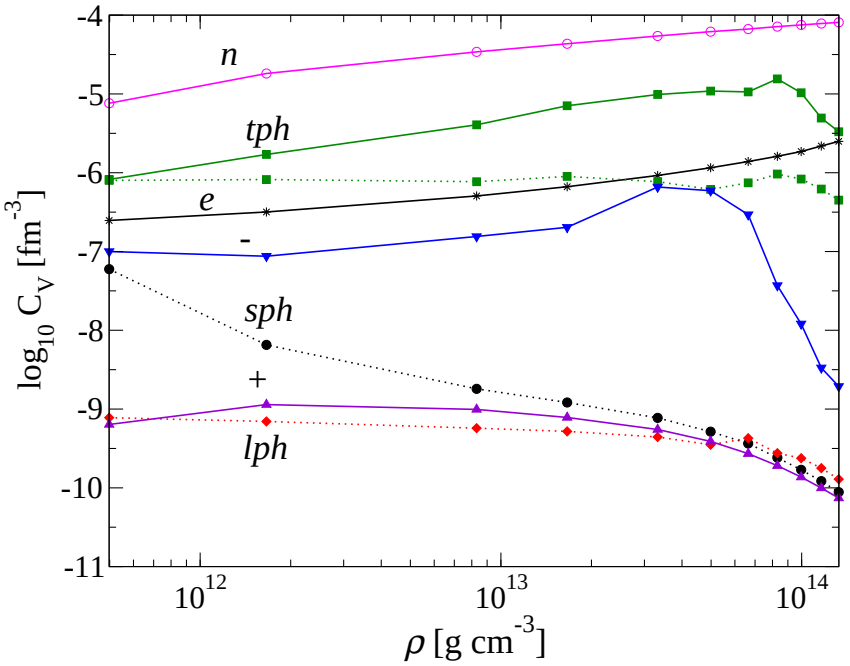

n normal neutrons
e electrons
tph transverse lattice phonons
lph longitudinal lattice phonons (without mixing)
sph superfluid phonons (without mixing)
$\pm$ longitudinal mixed modes

Entrainment and thermal properties

The contribution of collective excitations to the specific heat at low T varies like $(k_{\rm B}T/\hbar v)^3$. Since entrainment reduces v, the specific heat is enhanced.

Contributions to the crustal specific heat at $T = 10^9$ K :

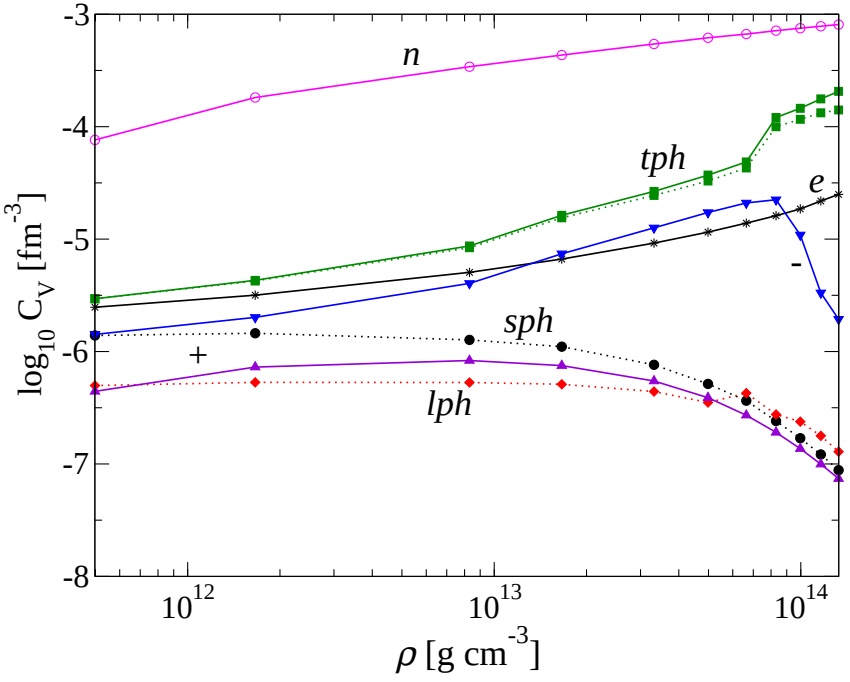

n normal neutrons
e electrons
tph transverse lattice phonons
lph longitudinal lattice phonons (without mixing)
sph superfluid phonons (without mixing)
$\pm$ longitudinal mixed modes

Entrainment and thermal properties

Changes in phonon velocities alter the electron-phonon scattering hence also the (electron) thermal conductivity.

All in all, entrainment leads to an increase of the thermal relaxation time of the crust.

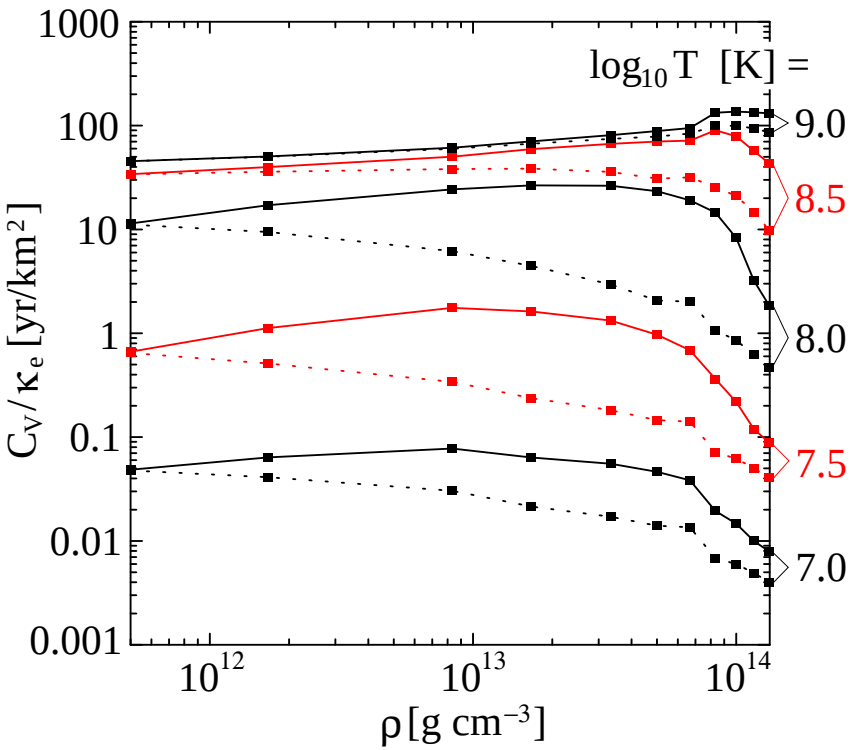

Thermal properties were calculated for catalyzed crusts; they may be different for accreted crusts.

Take home message

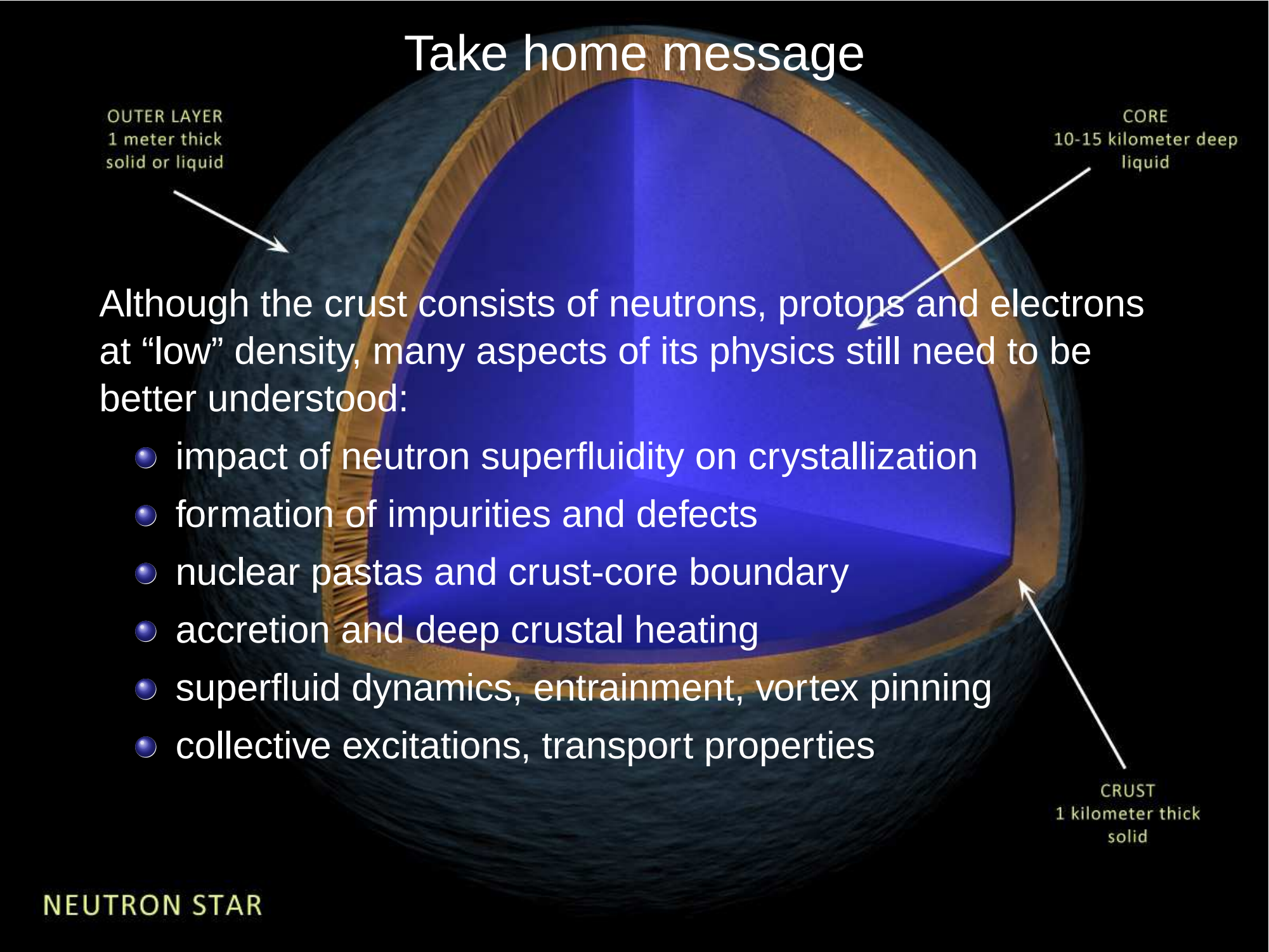

Although the crust consists of neutrons, protons and electrons at “low” density, many aspects of its physics still need to be better understood:

- impact of neutron superfluidity on crystallization
- formation of impurities and defects
- nuclear pastas and crust-core boundary
- accretion and deep crustal heating
- superfluid dynamics, entrainment, vortex pinning
- collective excitations, transport properties